A comprehensive two-hybrid analysis to explore the *L. pneumophila* effector-effector interactome

Harley O'Connor Mount[1]†, Malene L. Urbanus[2]†, Dayag Sheykhkarimli[3,4], Atina G. Coté[3,4], Florent Laval[5,6,7,8,9,10], Georges Coppin[5,6,7,9], Nishka Kishore[3,4], Roujia Li[3.4], Kerstin Spirohn-Fitzgerald[5,6,7], Morgan O. Petersen[2,11], Jennifer J. Knapp[3,4], Dae-Kyum Kim[3,4], Jean-Claude Twizere[8,9], Michael A. Calderwood[5,6,7], Marc Vidal[5,6], Frederick P. Roth[1,3,4,12] and Alexander W. Ensminger[1,2*]

[1]Department of Molecular Genetics, University of Toronto, Toronto, ON, M5G 1M1, Canada.

[2]Department of Biochemistry, University of Toronto, Toronto, ON, M5G 1M1, Canada.

[3]Donnelly Centre, University of Toronto, Toronto, ON, M5G 3E1, Canada.

[4]Molecular Genetics, Lunenfeld-Tanenbaum Research Institute, Toronto, ON, M5G 1X5, Canada.

[5]Center for Cancer Systems Biology (CCSB), Dana-Farber Cancer Institute, Boston, MA, 02215, USA.

[6]Department of Genetics, Blavatnik Institute, Harvard Medical School, Boston, MA, 02115, USA.

[7]Department of Cancer Biology, Dana-Farber Cancer Institute, Boston, MA, 02215, USA.

[8]TERRA Teaching and Research Centre, University of Liège, 5030, Gembloux, Belgium.

[9]Laboratory of Viral Interactomes, GIGA Institute, University of Liège, 4000, Liège, Belgium.

[10]Laboratory of Molecular and Cellular Epigenetics, GIGA Institute, University of Liège, 4000, Liège, Belgium.

[11]Department of Microbiology and Immunology, The University of Melbourne at the Peter Doherty Institute for Infection and Immunity, Melbourne, VIC 3000, Australia.

[12]Department of Computational and Systems Biology, University of Pittsburgh School of Medicine, Pittsburgh, PA, 15260, USA.

†These authors contributed equally to this work.

*Corresponding author:

Email: alex.ensminger@utoronto.ca

Running title:

A pathogen effector-effector interactome

Keywords: bacterial effector/host-pathogen/*Legionella pneumophila*/metaeffector/Yeast Two-Hybrid

Abstract

Legionella pneumophila **uses over 300 translocated effector proteins to rewire host cells during infection and create a replicative niche for intracellular growth. To date, several studies have identified** ***L. pneumophila*** **effectors that indirectly and directly regulate the activity of other effectors, providing an additional layer of regulatory complexity.** ***L. pneumophila*** **has the largest contingent of a new class of effectors, so called "metaeffectors" that directly regulate the activity of other effectors in the host. A defining quality of metaeffectors is the direct, physical interaction of the metaeffector with its cognate target effector. Metaeffectors identification to date has depended on phenotypes in heterologous systems, experimental serendipity and they represent only one class of physical interactions between effectors. Using a multiplexed, sequence-based yeast two-hybrid technology we screened the entire** ***L. pneumophila*** **effector proteome and components of the Dot/Icm type IV secretion system for protein-protein interactions (>167,000 protein combinations). Our screen captured 52 protein interactions, including 8 known and 44 novel protein interactions. Most notably, we identified ten novel effector-effector interactions, doubling the number of known effector-effector interactions.**

Introduction

Many bacterial pathogens actively translocate protein cargo, called ‘effectors’, into host cells to establish a replicative niche. The perspective that bacterial effectors exclusively target host pathways, and that effector activity is solely regulated by effector expression or translocation timing has been changing with the discovery of functional effector interactions in several bacterial pathogens (Kubori & Nagai, 2011; Shames & Finlay, 2012). The majority of effector interactions described to date are indirect antagonistic relationships, e.g. one effector antagonizes the action of another effector by acting on host targets. Some indirect antagonists compensate for negative side effects of other effectors (Dean *et al*, 2010) while others act on the same host factor with opposing actions such as by adding and removing post-translational modifications (Müller *et al*, 2010; Mukherjee *et al*, 2011; Neunuebel *et al*, 2011; Tan & Luo, 2011; Tan *et al*, 2011). Effectors in the latter class have the potential to regulate an action on the host in a spatial and/or temporal manner (Kubori & Galán, 2003). Cooperative effector interplay has also been identified such as the *Legionella pneumophila* paraeffectors LphD and RomA which work consecutively by first deacetylating and then methylating K14 of host histone 3 (Schator *et al*, 2023). Other effectors, such as LegC2, LegC3, and LegC7, directly cooperate–forming a SNARE-like complex with the human hVAMP4 protein to modulate membrane fusion (Shi *et al*, 2016). An emerging class of effectors, metaeffectors (“effectors of effectors”), do not target host proteins but instead directly bind to other effectors and regulate their activity once inside the host (Kubori *et al*, 2010; Magori & Citovsky, 2011; Joseph & Shames, 2021; Bastidas *et al*, 2024).

The intracellular pathogen *L. pneumophila* has the largest studied bacterial effector arsenal with over 300 effectors (Burstein *et al*, 2009; Huang *et al*, 2011; Zhu *et al*, 2011) and notably has several of such regulatory layers; indirect antagonist effectors (Müller *et al*, 2010;

Neunuebel *et al*, 2011; Mukherjee *et al*, 2011; Tan & Luo, 2011; Tan *et al*, 2011; Valleau *et al*, 2018; Gan *et al*, 2019a; Wan *et al*, 2019; Gan *et al*, 2020; Song *et al*, 2021), cooperative paraeffectors (Schator *et al*, 2023) and several metaeffectors (Kubori *et al*, 2010; Jeong *et al*, 2015; Urbanus *et al*, 2016; Shames *et al*, 2017; Valleau *et al*, 2018; Bhogaraju *et al*, 2019; Black *et al*, 2019; Gan *et al*, 2019b; Joseph *et al*, 2020; Hsieh *et al*, 2021; McCloskey *et al*, 2021; Song *et al*, 2021), including the effector LubX for which the term metaeffector was coined (Kubori *et al*, 2010). *L. pneumophila* is the causative agent of Legionnaires' disease (Fields *et al*, 2002) and uses the Dot/Icm Type IVB secretion system (T4SS) to deliver effectors to create a replicative niche in macrophages (Isberg *et al*, 2009) and protozoan species (Fields, 1996; Rowbotham, 1980; Molmeret *et al*, 2005; Faulkner *et al*, 2008; Watanabe *et al*, 2016; Boamah *et al*, 2017; Siddiqui *et al*, 2021). We previously used a genetic interaction screen in *Saccharomyces cerevisiae* to systematically identify *L. pneumophila* functional effector-effector regulation (Urbanus *et al*, 2016). Altogether, this approach identified twenty-three effector-effector suppression pairs, where an antagonist effector suppressed the yeast growth defect of a growth-inhibitory effector. We then examined this subset of effectors for protein-protein interactions (PPIs), using pairwise yeast two-hybrid and LUMIER, identifying nine instances of effector-effector interactions, a hallmark of metaeffectors. Collectively, our screen and other studies have identified 11 confirmed and putative metaeffectors in the *L. pneumophila* effector arsenal (Kubori *et al*, 2010; Jeong *et al*, 2015; Urbanus *et al*, 2016; Shames *et al*, 2017; Valleau *et al*, 2018). However, this is not a complete picture of the possible effector-effector interactions and regulatory pairs in this pathogen: for instance, effectors that do not have a conserved host target in yeast would have been missed in a genetic interaction screen due to a lack of growth inhibition. Similarly, the formation of a SNARE-like complex between LegC2, LegC3 and

LegC7 with hVAMP4 is a clear demonstration that physical interactions between effectors do not need to fall within the narrow scope of metaeffector-effector regulatory relationships (Shi *et al*, 2016).

To complement our previous genetic interaction screen, we performed a systematic screen for physical effector-effector interactions using the Barcode Fusion Genetic-Yeast Two-Hybrid (BFG-Y2H) assay, a high-throughput Y2H approach with a barcode sequencing readout (Yachie *et al*, 2016). Because many *L. pneumophila* effectors inhibit yeast growth when overexpressed (Campodonico *et al*, 2005; Shohdy *et al*, 2005; Heidtman *et al*, 2009; Guo *et al*, 2014; Urbanus *et al*, 2016), we modified the Y2H vectors to keep them transcriptionally silent prior to the readout of each potential binding event. This inducible BFG-Y2H (iBFG-Y2H) was used to screen 390 effectors and putative effectors and 28 Dot/Icm T4SS components in >167,000 pairwise combinations.

Results

Modification of a high-throughput yeast two-hybrid approach to reduce loss of yeast-toxic genes from screening libraries

To screen all *L. pneumophila* effectors for binary physical interactions, we performed a pooled, multiplexed yeast two-hybrid screen that relies on DNA barcoding to detect binary physical interactions within a library of clones (Yachie *et al*, 2016). Briefly, the BFG-Y2H assay is based on the original Y2H assay (Fields & Song, 1989) in which the yeast transcriptional activator Gal4 is split into a DNA-binding domain (DB) and an activating domain (AD). When these domains are fused to proteins that physically interact with each other, the Gal4 protein is reconstituted and drives transcription of reporter genes such as *GAL1::HIS3*, which allows for

growth on medium lacking histidine. In the BFG-Y2H assay, Y2H screens are performed in multiplexed pools using Illumina sequencing of molecular barcodes as a readout of the pool composition (Yachie *et al*, 2016) (Fig 1A). To identify the AD-DB combinations with Illumina sequencing, each vector contains a molecular barcode with two unique tags (up- and downtag) where one tag is flanked by unique lox sites (*loxP*, *lox2272*). The AD and DB barcoded vectors are pooled, transformed into yeast, mated *en masse* and the subsequent diploid pool is subjected to Y2H selection and control growth conditions. The lox-flanked tags on reciprocal AD and DB vectors within in the same cell are then recombined *in vivo* in the presence of Cre-recombinase. The resulting chimeric barcodes are unique for each AD and DB interaction pair and the abundance of these chimeric barcodes in the sequencing data reflects the abundance of the interaction pairs in the yeast pools (Yachie *et al*, 2016) (Fig 1A).

For the purpose of examining physical interactions between *L. pneumophila* effectors, one complication is that BFG-Y2H vectors contain the constitutive *ADH1* promoter, resulting in expression of AD and DB fused genes throughout the entire screening process. This poses issues for genes that impair yeast growth as strains expressing them are likely to be lost during library construction and expansion. Notably, two-thirds of *L. pneumophila* effectors are growth inhibitory ranging from severe to mild when expressed in yeast (Campodonico *et al*, 2005; Shohdy *et al*, 2005; de Felipe *et al*, 2008; Heidtman *et al*, 2009; Xu *et al*, 2010; Belyi *et al*, 2012; Guo *et al*, 2014; Nevo *et al*, 2014; Urbanus *et al*, 2016), which is likely due to the conservation of their targets in *S. cerevisiae* (Lesser & Miller, 2001; Campodonico *et al*, 2005; Shohdy *et al*, 2005; Heidtman *et al*, 2009; Xu *et al*, 2010; Tan *et al*, 2011; Belyi *et al*, 2012; Guo *et al*, 2014; Nevo *et al*, 2014; Dong *et al*, 2016; Liu *et al*, 2017; He *et al*, 2019).

To mitigate the impact of effector-induced growth inhibition, we modified each BFG-Y2H vector by replacing the constitutive *ADH1* promoter with the copper-inducible *CUP1* promoter (Butt & Ecker, 1987). In this way, we reasoned that expression of each DB- and AD-fusion could be silenced during library construction, expansion, and the mating of DB- and AD-containing strains. To confirm inducible expression of these vectors, we grew yeast with empty DB or AD vectors in medium lacking copper to keep expression at a minimum or induced with 1 mM copper for 3, 6 and 24 hours. We observed no expression of the AD and DB domain at T0 or when uninduced and increasing expression at 3, 6 and 24 hours (Fig 1B). Next, we tested five Y2H PPIs between antagonist and growth-inhibitory effectors that were identified previously by transformation of the AD-toxic effector fusions to strains already carrying their matched metaeffectors (antagonists) as DB fusions (Urbanus *et al*, 2016). Of these, four were captured using the inducible BFG-Y2H vectors without the need for co-transformations (Fig 1C). We observe a similar profile as in our previous assay (Urbanus *et al*, 2016), LegL1-RavJ and MavE-LegC7/YlfA were the strongest interaction pairs with robust growth on -Leu/Trp/His and the more stringent condition supplemented with 3-AT, an inhibitor of His3p. The weaker interaction LupA-LegC3 similarly only grew on -Leu/Trp/His medium, while SidP-MavQ in contrast to our previous findings did not grow on -Leu/Trp/His medium supplemented with 3-AT. Taken together, these data show that the inducible BFG-Y2H assay captures previously known metaeffector-effector pairs with a similar sensitivity profile.

An iBFG-Y2H screen of *L. pneumophila* Dot/Icm secretion system components and effectors

To extend this approach to the entire *L. pneumophila* effector arsenal (>300 proteins), we made a library of effectors and putative effectors in uniquely barcoded iBFG-Y2H vectors using a previously constructed Gateway collection (Losick *et al*, 2010; Urbanus *et al*, 2016) and included an additional 52 effectors and putative effectors (Table EV1). We also included 28 components of the Dot/Icm type IV secretion system (T4SS), both as positive controls and to investigate Dot/Icm protein interactions interact with effectors. As a positive reference set (PRS), we included 21 well-characterized human-human interaction pairs (Table EV2) (Yachie *et al*, 2016). Overall, these AD and DB fusion collections contain 435 unique open reading frames (ORFs) represented by 1,244 uniquely barcoded iBFG-Y2H vectors, and 422 unique ORFs represented by 1,137 uniquely barcoded iBFG-Y2H vectors, respectively (Table EV1). The majority of ORFs are represented by 3 unique barcode replicates (Fig EV1A, B). Of the 418 *L. pneumophila* effector and Dot/Icm ORFs, 400 are represented in both AD and DB libraries whereas the remaining 18 were only screened in one direction due to severe autoactivation and other technical limitations (Table EV3). We mated the AD and DB haploid collections *en masse* to generate a pool of AD-DB diploid cells (>1.4 million possible unique barcode combinations) and then induced expression using 1 mM copper during growth on control medium and selective medium lacking histidine. Following growth of the pools, the barcodes of the control condition and the Y2H selective condition were PCR amplified and Illumina deep sequenced (~54 and ~72 million read pairs, respectively). Each barcode recombination event results in two chimeric barcode combinations (Fig 1A, step 4, 5). To assess if there are barcode specific effects due to PCR or sequencing artifacts, we looked at the correlation of the two chimeric barcodes created during AD and DB barcode recombination for both pools (Fig EV1C, D), which showed a strong congruence indicating no major barcode specific effects.

Next, we benchmarked our screen by examining the barcode-fusion data for the 21 expected human-human interactions (Table EV2). For each possible AD-DB combination in the pool, an interaction score was calculated that reflects the enrichment of the AD-DB combination in the Y2H selective condition over the control condition (Fig 2A) (Yachie *et al*, 2016). At the maximum Matthews correlation coefficient (MCC), which optimizes precision and recall, 20 PRS interactions exceeded the MCC-optimal threshold (Fig 2B, Table EV4), a recall of 95%.

Outside of the hPRS set, 107 Dot/Icm-Dot/Icm, Dot/Icm-effector, effector-effector and human protein-effector interaction pairs exceeded the MCC-optimal threshold. To confirm these, we first recloned each gene and created individual AD and DB strains. After mating, the resulting diploids were spotted onto control medium and Y2H selective medium and scored for growth after 3 days. In total, this retesting confirmed 56 *L. pneumophila* interaction pairs (Fig 2C, Fig EV2, Table EV4), a confirmation rate of 52%. This is comparable to the ~50% retest rate of the original BFG-Y2H screen (Yachie *et al*, 2016) and other high-throughput Y2H studies (Rual *et al*, 2005; Yu *et al*, 2008; Simonis *et al*, 2009). Notably, we observed that as the confirmation series approached the MCC-optimal threshold, the Y2H retest-positive rate decreased rapidly, suggesting that the MCC-optimal threshold based on the hPRS is an appropriate cut-off for *L. pneumophila* interactions (Fig 2C).

Taken together, performance of the iBFG-Y2H screen in our hands matched prior expectations, capturing 95% of the human positive reference set and had a retest rate of 52% for the non-PRS interactions and captured 56 interaction pairs representing 52 unique PPIs (4 interactions were captured in both AD-DB orientations) (Table EV4).

Validation of iBFG-Y2H interactions by an orthologous (yN2H) assay

To further evaluate the quality of the *L. pneumophila* iBFG-Y2H interaction data, we next turned to the orthogonal yeast-based NanoLuc two-hybrid assay (yN2H) (Choi *et al*, 2019). In this assay, nanoluciferase is split into two fragments, the N-terminal Fragment 1 and C-terminal fragment 2. Enzymatic activity of NanoLuc is reconstituted when the two fragments are brought into close proximity by interacting fusion partners. We created copper-inducible N2H vectors to assay *L. pneumophila* PPIs in the yN2H assay. We measured the N2H signals of 33 retest-positive *L. pneumophila* interaction pairs as N1-X:N2-Y and N1-Y:N2-X fusions along with a set of well-described interactions (positive reference set, hsPRS-v2) and randomly selected pairs (random reference set, hsRRS-v2) (Venkatesan *et al*, 2009; Rolland *et al*, 2014; Choi *et al*, 2019; Luck *et al*, 2020) cloned into the standard N2H vector (Choi *et al*, 2019) (Table EV5). The detection rate for the *L. pneumophila* interactions pairs in a single orientation was compared to the detection rate of the hsPRS-v2 and hsRRS-v2 (Choi *et al*, 2019) (Fig 3A). The detection threshold was set at the NLR value where the hsRRS-v2 distribution has a Z-score >2.23 and the probability of the hsRRS-v2 values to be below the threshold is 98.7%. The validation rate of our dataset was 48.5 % which exceeds the hsPRS-v2 set validation rate of 18.3 % (Fig 3B). As such, the quality of the confirmed *L. pneumophila* iBFG-Y2H interactome exceeds that of a high-quality interaction dataset supported by multiple experiments in the curated literature (Braun *et al*, 2009; Venkatesan *et al*, 2009; Rolland *et al*, 2014; Choi *et al*, 2019; Luck *et al*, 2020).

The iBFG-Y2H screen identifies both known and novel Dot/Icm complex interactions

Turning to the biology of *L. pneumophila* interactions, we first looked at components of the Dot/Icm T4SS. The interaction score heatmap of the 27 DB- and 28 AD-fused Dot/Icm components present in the screen shows nine interaction pairs above the MCC-optimal threshold

and confirmed in the iBFG-Y2H retest assay (Fig 4A, Table EV4). We expected to see three interactions; IcmQ-IcmR (Duménil & Isberg, 2001), IcmS-IcmW (Coers *et al*, 2000; Ninio *et al*, 2005; Xu *et al*, 2017) and LvgA-IcmS (Vincent & Vogel, 2006; Kim *et al*, 2020), which have all been detected using several PPI assays, including the Y2H assay. IcmQ-IcmR and IcmS-IcmW were captured in both directions (Fig 4B) above the MCC-optimal threshold and confirmed in the iBFG-Y2H retest assay, but the LvgA-IcmS pairs were below the MCC-optimal threshold and were thus not further tested or validated. Of the five additional PPIs that confirmed in the iBFG-Y2H retest assay, three are supported by previously published data: DotB-DotB, IcmG/DotF-IcmG/DotF and DotC-IcmG/DotF (Fig 4B). The ATPase DotB can be purified as hexamer (Sexton *et al*, 2004), IcmG/DotF was shown to self-associate using the BACTH assay (Vincent *et al*, 2006) and DotC and IcmG/DotF are both part of the T4SS core complex (Vincent *et al*, 2006). The remaining two PPIs: IcmB/DotO-IcmT and IcmV-IcmG/DotF, are novel.

In contrast to a previous Y2H study identifying interactors of IcmW (Ninio *et al*, 2005), we did not identify any effector interactions with any of the components responsible for transferring effectors to the core transmembrane complex. This is the function of the Type IV coupling complex (T4CC) of which several components are present in the iBFG-Y2H library (IcmO/DotL, IcmP/DotM, IcmJ/DotN, DotY, IcmS, IcmW and LvgA) (Vincent *et al*, 2012; Sutherland *et al*, 2012; Kwak *et al*, 2017; Xu *et al*, 2017; Meir *et al*, 2018, 2020). However, we did find interactions of effectors with Dot/Icm components that are part of the core complex spanning the inner membrane, periplasm and outer membrane: IcmG/DotF, IcmN/DotK, IcmE/DotG and DotC (Fig 4C) (Vincent *et al*, 2006; Ghosal *et al*, 2019; Durie *et al*, 2020). Notably, IcmG/DotF was previously shown to interact with effectors in BACTH assays (Luo &

Isberg, 2004; Sutherland *et al*, 2013) though the relevance of these interactions is unclear (Sutherland *et al*, 2013).

Taken together, we captured several known interactions from the Dot/Icm T4SS, uncovered two novel Dot/Icm interactions: IcmB/DotO-IcmT, IcmV-IcmG/DotF and several effector-Dot/Icm T4SS interactions.

iBFG-Y2H identifies several novel effector-effector interactions

Next, we looked at effector and putative effector interactions that confirmed in the iBFG-Y2H retest assay (Fig 5). The screen captured eleven effectors that dimerize (Fig 5A), of which only WipA had previously been shown to dimerize (Pinotsis & Waksman, 2017). Beyond this, we identified thirteen physical interactions between pairs of distinct effectors (Fig 5B). These include the published effector-metaeffector pairs RavJ-LegL1 (in both directions) and LegC7/YlfA-MavE (Urbanus *et al*, 2016), consistent with the results of our pilot experiment (Fig 1C). Ten PPIs are novel effector-effector pairs. Of these, three contain a core (conserved) effector–RavC, CetLP1 or Lpg2832 (Burstein *et al*, 2016; Gomez-Valero *et al*, 2019)–and three have at least one effector with some characterization–Lpg2149-VipA (Franco *et al*, 2012; Bugalhão *et al*, 2016; Valleau *et al*, 2018), PieF-LegK2 (Hervet *et al*, 2011; Michard *et al*, 2015; Mount *et al*, 2022) and WipA-Lpg2860 (He *et al*, 2019; Jia *et al*, 2018; Pinotsis & Waksman, 2017). The remaining four pairs identified in our screen consist of completely uncharacterized effectors and putative effectors.

An incidental consequence of the human PRS: identification of several effector-host interactions

While our screen focused on effector-effector interactions, one consequence of using a set of evolutionary conserved human proteins to benchmark a pooled interaction screen was the fortuitous scoring of interactions between effectors and these conserved host proteins. Several proteins of the human PRS, which contains conserved eukaryotic proteins such as proteins involved in cell cycle regulation or mRNA degradation, were also found to interact with *L. pneumophila* effectors. We identified 17 effector-human protein pairs: 8 effectors interact with transcription factor Ikaros (IKZF1) (Fig 6A) and the remaining 9 pairs involve 6 different effectors and 7 human proteins (Fig 6B). Of these interactions, 16 are novel and only the PieF-CNOT7 interaction was reported previously (Mount *et al*, 2022).

A high-confidence effector interaction network

Using iBFG-Y2H, two novel Dot/Icm-Dot/Icm interactions, six novel effector-Dot/Icm interactions, ten novel effector dimers, ten novel effector-effector interactions and 17 novel effector-human protein interactions were identified. These PPIs and previously published PPIs captured in the iBFG-Y2H screen are visualized in a network (Fig 7), where nodes of published interactions are coloured blue. Examination of this network shows that while most effectors only interact with one other effector or human protein, a few effectors standout as interacting with several different proteins: PieF (interacting with IKFZ1, CNOT7, CDK4, LSM3 and LegK2), VipA (with CDK4 and Lpg2149), Lpg2885 (with Lpg1822 and CetLP1) and MavA (with IKZF1, MRFAP1L1 and AVR58-05830).

Discussion

With over 300 effectors, *L. pneumophila* has the largest described bacterial effector arsenal (Ensminger, 2016) and several examples of effector interplay that finetune effector function and the progression of pathogenesis (Kubori *et al*, 2010; Müller *et al*, 2010; Neunuebel *et al*, 2011; Tan *et al*, 2011; Tan & Luo, 2011; Mukherjee *et al*, 2011; Jeong *et al*, 2015; Urbanus *et al*, 2016; Shames *et al*, 2017; Valleau *et al*, 2018; Gan *et al*, 2019a; Wan *et al*, 2019; Gan *et al*, 2020; Schator *et al*, 2023). We previously performed the first genetic interaction screen of bacterial effectors, where we expressed every possible combination of *L. pneumophila str. Philadelphia* effectors in the budding yeast *S. cerevisiae* and identified several suppression pairs, where an antagonist effector suppresses the yeast-growth defect of a yeast growth-inhibitory effector (Urbanus *et al*, 2016). These suppression pairs were enriched for metaeffectors, effectors that directly target other effectors and regulate their activity in the host cell. Collectively, the field has identified 11 *L. pneumophila* metaeffectors to date (Kubori *et al*, 2010; Urbanus *et al*, 2016; Shames *et al*, 2017; Valleau *et al*, 2018). We reasoned that our genetic interaction screen did not capture all metaeffectors or effectors functioning in a complex (Shi *et al*, 2016). To complement our previous work, we set out to screen all possible effector-effector physical interactions using iBFG-Y2H, a high-throughput, multiplexed protein interaction screen with inducible expression and barcoded vectors for a sequencing readout.

In this study, we present the systematic physical interaction screen of a large bacterial pathogen effector arsenal for effector-effector interactions, encompassing 390 *L. pneumophila* effectors and putative effectors, 28 Dot/Icm components. We identified 52 interactions between *L. pneumophila* effectors, Dot/Icm T4SS components and effectors with Dot/Icm T4SS components or human proteins. A subset of confirmed iBFG-Y2H PPIs were validated in the orthologous NanoLuc Two-Hybrid (N2H) assay (Choi *et al*, 2019) with a validation rate of

48.5% (Fig 3), indicating the confirmed iBFG-Y2H set is high-confidence dataset with 16 PPIs captured in two assays. Indeed, our screen captured several known interactions between components of the Dot/Icm T4SS system (Coers *et al*, 2000; Duménil & Isberg, 2001; Sexton *et al*, 2004; Ninio *et al*, 2005; Vincent *et al*, 2006; Xu *et al*, 2017; Kim *et al*, 2020), the WipA dimer (Pinotsis & Waksman, 2017) two of our previously published effector-metaeffector pairs; RavJ-LegL1 and LegC7/YlfA-MavE (Urbanus *et al*, 2016) and PieF-CNOT7 (Mount *et al*, 2022) (Fig 7). The novel ten effector-effector interactions involve 19 effectors, approximately 5% of the total effectors, and more than doubles the number of effector-effector PPIs previously detected by a Y2H assay. This reinforces the notion that bacterial effectors do not act on their own and need to be studied in concert rather than in isolation.

The functional consequences of the effector interactions we observe remain to be defined. They may represent metaeffector-effector pairs, effectors functioning in a complex, or some other functional relationship yet to be discovered. However, these physical interactions suggest interesting functional links. For example, Lpg2149 links the actin nucleator VipA (Franco *et al*, 2012) with modulators of the E3 ubiquitin ligase UBE2N, MavC and MvcA, where MavC modifies and inactivates UBE2N (Valleau *et al*, 2018; Gan *et al*, 2019a, 2020) and MvcA removes that modification (Gan *et al*, 2020; Wang *et al*, 2020). Lpg2149 is the metaeffector of MavC and MvcA inactivates both effectors (Valleau *et al*, 2018). Notably, UBE2N has been shown to be involved in ubiquitination of β-actin (Chua *et al*, 2018) and was recruited to actin-rich structures in *Listeria monocytogenes* infections (Chua *et al*, 2023).

A fortuitous consequence of including the human positive reference set in our screen was the detection several novel host protein-effector interactions. The transcription factor Ikaros (IKZF1) stands out as it interacts with a striking number of effectors. Ikaros is involved, amongst

others, in regulation of the host response to bacterial LPS (Oh *et al*, 2018) and hypomorphic Ikaros alleles leave patients at high risk for viral and bacterial infections (Kuehn *et al*, 2022). This raises the question of whether one or more of these effectors modulate Ikaros-regulated host defenses. Notably, *L. pneumophila* has been shown to target other immune related transcription factors such as NF-κB (Ge *et al*, 2009; Losick *et al*, 2010). In our screen we also find that the effector Ceg29 interacts with PSMD2, the proteasome non-ATPase regulatory subunit 2 (TRAP2), which can bind to TNF receptor and is implicated in TNF signalling, a signalling pathway known to restrict *L. pneumophila* growth (Liu *et al*, 2008; Pollock *et al*, 2023). Two other human protein-effector PPIs that can be linked to known processes during *L. pneumophila* infection are 1. AP2B1-Lem2 and 2. SH3GLB2 (Endophillin B2)-Ceg7. AP2B1 is a component of the clathrin adaptor complex, AP2, and is involved in endocytosis, while Endophillin B2 facilitates endosome maturation. Both of these processes are heavily targeted by *L. pneumophila* as it evades host defenses and maturation of the host phagosome (Finsel & Hilbi, 2015). Interestingly, the AP2 complex is also targeted by an effector of *Coxiella burnetii* (Larson *et al*, 2013) a bacterial pathogen with a intracellular lifestyle related to *L. pneumophila*. Finally, during infection *L. pneumophila* blocks the host cell cycle progression in an effector dependent manner (Mengue *et al*, 2016; Sol *et al*, 2019). Two effectors, VipA and PieF, were found to interact with the cyclin dependent kinase CDK4 suggesting that they could be involved in cell cycle regulation.

In summary, our iBFG-Y2H screen of all *L. pneumophila* effectors captured a novel set of PPIs, which builds on and expands knowledge of the molecular interactions between *L. pneumophila* effectors that facilitate the pathogenesis program of *L. pneumophila*. Our dataset doubles the number of known effector-effector interactions and shows that effector-effector

interactions and effector interplay are common, rather than an exception. The next steps in studying these interactions, such as investigating the role of these interactions during host infection, will undoubtedly lead to novel biology and a greater understanding of regulation of pathogenesis of intracellular bacterial pathogens.

Methods

Strains and culture conditions

Escherichia coli strain Top10 was used for cloning and plasmid production and grown in LB Miller or 2X LB Miller. *S. cerevisiae* strains RY1010 (MATa *leu2-3,112 trp1-901 his3-200 ura3-52 gal4Δ gal80Δ PGAL2-ADE2 LYS2::PGAL1-HIS3 MET2::PGAL7-lacZ cyh2^R can1Δ::PCMV-rtTA-KanMX4)*, RY1030 (*MATα leu2-3,112 trp1-901 his3-200 ura3-52 gal4Δ gal80Δ PGAL2-ADE2 LYS2::PGAL1-HIS3 MET2::PGAL7-lacZ cyh2^R can1Δ::TADH1-PtetO2-Cre-TCYC1-KanMX4*) (Yachie *et al*, 2016), Y8800 (MATa) and Y8930 (MAT*α*) (genotype: *leu2-3,112 trp1-901 his3-200 ura3-52 gal4Δ gal80Δ PGAL2-ADE2 LYS2::PGAL1-HIS3 MET2::PGAL7-lacZ cyh2^R)* were grown in YPAD medium (2% bacto peptone w/v, 1% yeast extract w/v, 2% glucose v/v, 180 mg/l adenine) or synthetic complete (SC) medium lacking specific amino acids with 2% glucose and 180 mg/l adenine. The SC medium for copper inducible strains was prepared using yeast nitrogen base (YNB) without amino acids or copper (ForMedium, cat nr CYN0905).

Inducible BFG-Y2H vectors

The constitutive *ADH1* promoter in the BFG-Y2H vectors pNZM1090 and pNZM1100 (Yachie *et al*, 2016) was replaced with the *CUP1* promoter sequence (Butt & Ecker, 1987). The HindIII

site in the *TRP1* gene of pNZM1090 was removed by QuikChange (Agilent) per manufacturer's instructions using primers pNZM1090F and pNZM1090R (Table EV6). The *CUP1* promoter was amplified from *S. cerevisiae* BY4741 genomic DNA (Brachmann *et al*, 1998) using primers AE897 and AE898, the resulting PCR product was digested with ApaI/HindIII and ligated into ApaI/HindIII digested pNZM1090 and pNZM1100. The resulting vectors pNZM1090CUP1 and pNZM1100CUP1 were sequence verified.

Inducible expression was tested by growing RY1010 pNZM1090CUP1 and RY1030 pNZM1100 strains on SC medium lacking tryptophan or leucine, respectively. Overnight cultures were diluted to 1 OD_{600nm}/ml and induced with or without 1 mM $CuSO_4$. Three OD_{600nm} units were harvested at 0, 3, 6 and 24 h. Samples were lysed as described previously (Zhang *et al*, 2011) and resuspended in 100 µl 2X sample buffer (4% SDS, 20% glycerol, 120 mM Tris pH6.8). The equivalent of 0.3 OD units was analyzed by SDS-PAGE and western blot using the following antibodies and dilutions: mouse anti-AD (Abcam, cat nr ab135398) 1:200 in 3% BSA in PBS-0.5% Tween (PBS-T), mouse anti-DB (Abcam, cat nr ab135397) 1:1000 in 3% BSA in PBS-T, rabbit anti-actin (MilliporeSigma, cat nr A2066) 1:2500 in 5% milk PBS-T and secondary antibodies anti-mouse HRP (1:5000 for anti-AD, and 1:10,000 for anti-DB in 5% milk PBS-T) and anti-rabbit HRP (1:10,000 in 5% milk PBS-T) (Cell Signalling Technology, cat nrs 7076 and 7074).

Barcoded iBFG-Y2H plasmid collection

Randomly barcoded iBFG-Y2H vectors were made as described previously (Yachie *et al*, 2016) with the modification that the barcode cassette was inserted at the SacI site downstream of the Gateway cassette.

A Gateway pDONR221 library containing confirmed and putative *L. pneumophila* effectors described previously (Losick *et al*, 2010; Urbanus *et al*, 2016) was a kind gift from Dr. Ralph Isberg. We cloned an additional 52 effectors and putative effectors and 26 Dot/Icm components. ORFs were amplified from genomic DNA from *L. pneumophila* strain Lp02 (Rao *et al*, 2013) using the primers listed in Table EV6. The PCR products were cloned into pDONR221-ccdB (Invitrogen) using Gateway BP clonase II (Invitrogen) per manufacturer's instructions and the resulting vectors were sequence verified. The pDONR221 library was cloned *en masse* using Gateway LR Clonase II (Invitrogen) into randomly barcoded iBFG-Y2H vectors. A set of 34 human ORFs (Table EV2) for calculation of precision, recall and Mathew's correlation coefficient (MCC) values was included as described (Yachie *et al*, 2016).

The randomly barcoded pools were transformed into chemically competent Top10 *E. coli* cells and transformants were arrayed in 384-well format using an S&P robotic rearrayer (S&P Robotics). Barcode and ORF sequences for each clone were determined by kiloSEQ (seqWell Inc). Up to three independent clones were chosen for each ORF. Missing ORFs were cloned individually into randomly barcoded iBFG-Y2H vector pools and transformed into Top10 *E. coli*, and six clones were selected and arrayed into 96-well plates. The barcodes were sequenced using pooled Illumina sequencing with row-column-plate barcodes to link vector barcodes to a unique plate and well identity. Briefly, *E. coli* cultures were grown overnight in LB medium with 100 μg/ml carbenicillin at 37ºC with shaking in 96-well plates and diluted 1/20 in ddH_2O. Ten microliter row-column PCR reactions were performed with 1 μl barcoded primer corresponding to row A-H and 1 μl barcoded primer for column 1-12 barcoded primer (oHM106-199) (2 μM stock), 5 μl of KAPA HiFi 2X master mix (Roche) and 3 μl of diluted overnight culture grown in 96-well plates. Following PCR amplification, the amplicons from a 96-well plate are pooled

and purified using a 2% E-Gel SizeSelect II agarose gel (Invitrogen) and quantified on a NanoDrop spectrophotometer (ThermoFisher Scientific). Purified amplicon pools then underwent a second PCR amplification adding Illumina flow cell adapters as well as additional inline plate barcode sequences (primers oHM146-147, oHM200-213). For each plate, a 40 µl KAPA HiFi reaction was assembled using 1 µl of each primer (oHM200-213, 10 µM stock) and 5 µl of amplicons (1 ng/µl) and purified as above. The purified products were quantified using the NEBNext Library Quant kit for Illumina (NEB) and sequenced using a mid-output reagent cartridge with 2x150 paired-end reads on an Illumina Miniseq platform. Reads were demultiplexed using a custom Perl script (Yachie *et al*, 2016) and aligned to vector sequence using BLAST+ (Camacho *et al*, 2009) to extract barcode identities. Up to three independent clones were selected for each ORF. Plasmid pools were purified from the final arrayed *E. coli* collections using PureYield Plasmid Midipreps (Promega).

iBFG-Y2H screen

The iBFG-Y2H screen was performed using the *S. cerevisiae* BFG-Y2H toolkit strains RY1010 and RY1030 strains (Yachie *et al*, 2016). Frozen competent yeast cells prepared as described (Gietz & Schiestl, 2007a) and transformed as follows, 2 ml of frozen competent RY1010 or RY1030 cells were thawed, pelleted and resuspended in an 8.280 ml yeast transformation mixture (33% PEG3350, 0.1 M lithium acetate, 0.3 mg/ml boiled salmon sperm DNA) with 40 µg of the AD or DB iBFG-Y2H vector pool and heat-shocked at 42ºC for 1 h. The cells were pelleted at 1000x*g* for 5 min, washed once with 10 ml ddH_2O, re-suspended in ~ 1ml ddH_2O and plated on eight 15 cm plates of SC medium lacking tryptophan (-Trp for AD vectors), or lacking leucine (-Leu for DB vectors) without copper. Transformants were grown at 30ºC for 3 days,

before being scraped from the plates with ddH_2O and pooled. AD and DB pools were pelleted, washed twice with 25 ml of ddH_2O and resuspended to 100 OD_{600nm} units/ml. To mate, equal volumes (30 ml) of the AD and DB pools were combined and incubated for 3 h at room temperature (RT) without shaking (Bickle *et al*, 2006). The cells were pelleted, resuspended in 1.5 ml of ddH_2O and plated on ten 15 cm YPAD plates and incubated at RT for 3 days. The mated yeast pool was scraped, pelleted and washed twice and resuspended in ddH_2O to 50 OD_{600nm}/ml. The mated pool was plated on eighteen 15 cm plates (200 µl per plate) of Y2H selective media (SC-Leu/Trp/His + 1 mM $CuSO_4$), as well as diploid selective media (SC-Leu/Trp) supplemented with 1 mM $CuSO_4$ and 8 mM excess of histidine, and incubated at 30ºC for 3 days. For each condition, the plates were then scraped, pooled, washed twice with ddH_2O, and diluted to 1 OD_{600nm}/ml in 100 ml of diploid selective media without $CuSO_4$ and with 10 µg/ml of doxycycline to induce Cre-recombinase expression. To allow *in vivo* Cre-mediated recombination of barcodes the culture was grown overnight at 30ºC with 200 rpm shaking until the OD_{600nm} exceeded 5. Plasmids pools were isolated using the Zymoprep II yeast plasmid miniprep kit (Zymo Research). The fused DNA barcode sequences were amplified using KAPA HiFi 2x master mix and fusion specific primer pairs for each treatment (oHM380-387). For each condition twenty 40 µL reactions were run with 2 ng of DNA template per reaction to reduce sampling error and pooled together. The primers were used at 10 µM and contained adapters for the Illumina flow cell as described (Yachie *et al*, 2016). The PCR amplicon pools were then purified using 0.7X AMPure magnetic beads (Beckman Coulter) following the Illumina NexteraXT recommendations. The concentration of the purified amplicons was quantified by qPCR using the NEBNext Illumina Quant kit (NEB). The forward and reverse reads were demultiplexed and fused barcodes were quantified through alignment against custom barcode

and primer sequences using Bowtie2 (V2.3.4.1) (-q –local –very-sensitive-local -t -p 23 -reorder) (Langmead & Salzberg, 2012).

Interaction score calculation

Interaction scores were calculated as described previously (Yachie *et al*, 2016). Briefly, (i) a constant value of 1 was added to every AD-DB barcode combination in both the selective (-Leu/Trp/His + 1 mM $CuSO_4$) and non-selective (-Leu/Trp + 1 mM $CuSO_4$/8 mM His) matrices. (ii) The marginal frequency of each AD or DB clone within the population was determined by dividing the sum of barcode counts for all clones that contain that barcode in the non-selective condition by the sum of all barcode counts in the non-selective matrix. The expected frequency of any AD-DB combination is the product of each clone's marginal frequency in the non-selective condition. (iii) To score enrichment in the selective condition, the frequency of each AD-DB combination was calculated by dividing barcode count for every AD-DB combination by the sum of all barcode counts in the selective matrix. Raw score values (S) were then determined by dividing the selective frequency by the expected marginal frequency product determined in (ii). (iv) Autoactivation was normalized across each DB clone. First, the median value of all S values for each DB clone was subtracted from each raw score (S) giving a new value (S^o). S^o was then divided by the S value that encompasses 60% of all interactions for that DB clone resulting in the interaction score S'. For each AD-DB pair multiple S' scores were calculated based on the number of barcodes for each clone in the pool and the two chimeric barcodes for each AD-DB combination. Through systematic determination, we found that the optimal Matthews Correlation Coefficient (maximizing precision and recall) where MCC

optimal = 0.9 was achieved with a threshold where the top 60% of interactions were included in the normalization (ρ=0.4) and the average of the top 8 S' signals was adopted.

Pairwise retesting of iBFG-Y2H candidate interactions.

Of the 140 PPI pairs above the MCC-optimal rank, we retested 107 pairs involving Dot/Icm-Dot/Icm pairs, effector-Dot/Icm pairs, effector-effector pairs and effector-human protein pairs. Validated Gateway Entry clones were recloned into unbarcoded pNZM1090CUP1 and pNZM1100CUP1 vector using Gateway LR Clonase II (Life Technologies) per manufacturer's instructions. The resulting vectors were transformed to RY1010 and RY1030 as described (Gietz & Schiestl, 2007b) and grown for 2 days at 30°C on SD-Trp or SD-Leu agar plates. The resulting haploid strains were arrayed in a 96-well format as an DB (RY1030 pNZM1100CUP1) and AD (RY1010 pNZM1090CUP1) array. Using the S&P pinning robot (S&P robotics) the DB and AD arrays were pinned together on YPAD agar plates, incubated overnight at 30°C and diploid strains carrying both plasmids were pinned on SD-Leu/Trp agar plates and grown for 2 days at 30°C. An empty vector control was included on each array plate. To check for autoactivator activity, the DB and AD arrays were mated to an AD or DB empty vector control strain, respectively. The resulting diploid plates were grown overnight in 100 µl SD-Leu/Trp medium in 96-well plates at 30°C, diluted 10-fold in fresh medium and spotted on SD-Leu/Trp (control), SD-Leu/Trp/His -/+ 1 mM 3-AT (Y2H selective conditions) agar plates using a 96-well pin tool (V&P404, V&P Scientific) and grown for 3 days at 30°C before imaging (Fig EV2, Table EV4).

Pairwise validation of L. pneumophila effector interactions by yN2H assay

The promoter sequence of the NanoLuc Two-Hybrid (N2H N1 & N2) vectors (Choi *et al*, 2019) was replaced with the *CUP1* promoter. The *CUP1* promoter sequence was amplified from the iBFG-Y2H vectors (primers oHM487/488) and cloned into N2H N1 and N2 vectors digested with SpeI/SacI using NEBuilder assembly (NEB) according to manufacturer's instructions. The resulting vectors pHM526 and pHM527 were Sanger sequence verified.

ORFs from the iBFG-Y2H confirmed set were cloned into iN2H pDEST vectors using LR Clonase II as described above. Bacterial transformants were grown overnight in LB + carbenicillin (100 µg/ml), 200 µl of culture was pelleted and resuspended in 130 µl. Fifteen microliters of cell suspension was incubated for 30 min at 27ºC with 15 µl of 2x bacterial lysis buffer (2 mg/ml lysozyme, 20 mM Tris-HCl pH 6.8, 2 mM EDTA). The lysates were incubated for 20 mins at 55ºC with 5 µl of proteinase K mixture (12 mg/ml proteinase K, 20 mM Tris-HCl, 2 mM EDTA) followed by 20 mins at 80ºC to inactivate proteinase K. Competent yeast cells (Y800 and Y8930) were prepared as described (Gietz & Schiestl, 2007b) 20 µl of competent Y8800 or Y8930 cells was pelleted, resuspended in 148 µl of yeast transformation mix and combined with 15 µl of lysate for transformation. Transformations were incubated for 30 mins at 42ºC, pelleted and resuspended in 100 µl of YPAD. Resuspended yeast cells were recovered for 2 h at 30ºC washed with 100 µl of ddH_2O, resuspended in 10 µl of ddH_2O, plated onto selective media (SC-Leu or SC-Trp) and incubated for 3 days at 30ºC.

The yN2H assay was performed as described (Choi *et al*, 2019) with minor modifications. Briefly, Y8930 with pHM526 (N1/Fragment 1, *LEU2* cassette) or Y8800 + pHM527 (N2/Fragment 2 vectors, *TRP1* cassette) were grown overnight in 160 µl SC-Leu or SC-Trp medium at 30°C in a 96-well plate. A positive and random reference set (hsPRS-v2 and hsRRS-v2) in original N2H vectors (Choi *et al*, 2019) were grown in parallel. Two protein pairs

from the hsPRS-v2 (SKP1-SKP2; NCBP1-NCBP2) were included in duplicate on every test plate and used as positive controls. Mating was performed by mixing 5 µl of each Y8930 and Y8800 strain in a 96-well plate containing 160 µl YPD medium per well and incubated overnight at 30ºC. Strains expressing *L. pneumophila* ORF fusions were also mated with a control strain expressing only Fragment 1 (N1) or Fragment 2 (N2) to measure the background signal (e.g. N1-X was mated with N2-Y, where X and Y are the proteins tested for interaction, as well as Fragment 2 alone). To select for diploid strains, 10 µl of the mating mixture was grown overnight in 160 µl SD-Leu/Trp at 30°C in 96-well plates. Fifty microliters of the diploid selection cultures were transferred into 1.2 ml of fresh medium (SC-Leu/Trp) in deep 96-well plates. Plates were grown overnight at 30ºC with shaking, cultures were pelleted (1,800xg for 15 min) and resuspended in 100 µl NanoLuc Assay solution (Promega). The homogenized cell suspensions were transferred into white flat-bottom 96-well plates and incubated for 1 h at RT while protected from light. The luminescence signal was measured using a TriStar2 LB 942 luminometer (Berthold) with a one-second orbital shake before each measurement and an integration time of 2 s per sample.

For each protein pair X-Y, we calculated a normalized luminescence ratio (NLR) corresponding to the raw luminescence value of the tested pair (X-Y) divided by the maximum luminescence value from one of the two controls (X-Fragment 2 or Fragment 1-Y) (Choi *et al*, 2019). The log-transformed normalized luminescence ratio (NLR) was plotted for the human PRS (hsPRS-v2), RRS (hsRRS-v2), and confirmed iBFG-Y2H pairs (lpPPIs). Fraction detected, and confidence clouds (68.3% Bayesian confidence interval) were calculated at each NLR score threshold. Instead of establishing a detection threshold solely reliant on the hsRRS-v2 pair with the maximum NLR (Choi *et al*, 2019), we opted to derive the threshold from the entire

distribution of hsRRS-v2 scores. Specifically, we selected a Z-score threshold of 2.23, aligning with the next non-null detection value for a dataset size of 78, corresponding to a 1/78 hsRRS-v2 detection rate.

iBFG-Y2H analysis and data availability

Analysis scripts, resource files, and raw data can be accessed at https://github.com/EnsmingerLab/iBFG-Y2H.

Acknowledgements

We thank members of the Roth lab, Marinella Gebbia for assistance with library construction, Jochen Weile, Natascha van Lieshout, Anjali Gopaland and Nozomu Yachie for bioinformatic advice. Finally, we thank members of the Ensminger lab, Veronique Cartier-Archambault and Guangqi Zhou for help with cloning, Beth Nicholson, Jordan Lin and John McPherson for their suggestions and careful reading of the manuscript.

Funding

This work was supported by a Project Grant (AWE) from the Canadian Institutes of Health Research (PJT-162256). HOM was supported by a CGS-D fellowship from the Natural Sciences and Engineering Research Council of Canada. This work was also supported by a Wallonia-Brussels International (WBI)-World Excellence Fellowship (FL, GC), a Fonds de la Recherche Scientifique (FRS-FNRS)-Télévie Grant (FC31747, Crédit n° 7459421F) (FL, J-CT), the Fondation Léon Fredericq (FL and J-CT), a University of Liège mobility grant (FL), a Fonds de la Recherche Scientifique (FRS-FNRS) Mobility and Congress funding (n°40020393) (FL), a

Josée and Jean Schmets Prize (FL), a Herman-van Beneden Prize (FL), and a Fonds de la Recherche Scientifique (FRS-FNRS)-Fund for Research Training in Industry and Agriculture (FRIA) Grant (FC31543, Crédit n° 1E00419F) (GC). MV is a Chercheur Qualifié Honoraire and J-CT is a Maître de Recherche from the Fonds de la Recherche Scientifique (FRS-FNRS, Wallonia-Brussels Federation, Belgium).

Author contributions

MLU and AWE conceived and designed the screen for effector-effector interactions. HOM constructed the library and performed the iBFH-Y2H screen with assistance and training from AGC, DS, and MLU. En masse Gateway cloning was performed by MLU, AGC, NK, and RL, with subsequent robotic cherry-picking by AGC, NK, RL, DK and JK. Library sequencing was performed by HOM, DS, AGC, NK, and RL. HOM and MLU analyzed the data with assistance from DS. MLU performed the Y2H confirmation experiments, MOP assisted MLU with data analysis and network visualization. FL performed the yN2H validation experiment with assistance from KSF. GC analyzed the yN2H data. MC, JCT, MV, FPR, and AWE provided project supervision and advice. MLU and AWE with input from other authors prepared the manuscript.

Competing interests

F.R. and M.V. are advisors and shareholders of SeqWell, Inc. (Beverly, MA, USA).

Figure legends

Figure 1: inducible BFG-Y2H

A Schematic representation of the iBFG-Y2H screen. 1: All AD and DB vectors carry a unique molecular barcode consisting of an uptag and a downtag of which one is flanked by lox sites (*loxP*, *lox2272*; grey and black bar). 2: Haploid yeast pools with unique barcoded AD and DB clones are mated *en masse* and grown on medium lacking tryptophan and leucine to select for diploid cells carrying all combinations of the AD and DB vectors. 3: The diploid pool is grown on control and Y2H selective conditions with 1 mM $CuSO_4$ to induce expression of the AD and DB fusions. AD and DB fused proteins that interact with each other reconstitute the function of the Gal4p transcription factor and drive expression of the reporter gene *GAL1::HIS3*, allowing growth on Y2H selective medium. 4: After induction of Cre-recombinase expression, the AD downtag and DB uptag recombine with each other in each cell, creating two chimeric barcodes that represent the combined identities of the AD and DB vectors in those cells. 5: The chimeric barcodes are PCR amplified using primers containing Illumina adaptor sequences. 6: Illumina deep sequencing gives the abundance of each unique chimeric barcode, which reflects the abundance of the cells carrying those specific AD-DB combinations in the control or Y2H selection pool. This abundance in turn reflects, in the Y2H selection condition, the interaction between the AD and DB fusion partners.

B Test of the *CUP1* promoter in the AD and DB vectors. Empty AD and DB vectors were grown on medium lacking copper, backdiluted and grown with and without 1 mM $CuSO_4$. Samples were taken at 0, 3, 6 and 24 h, analyzed on SDS-PAGE and immunoblotted using anti-AD, anti-DB and anti-actin as a loading control.

C An inducible Y2H assay using known Y2H interaction pairs between yeast growth inhibitory *L. pneumophila* effectors (bold and underlined) and their antagonist effectors (Urbanus *et al*, 2016) and empty vector controls (EV). Strains were spotted on control (-Leu/Trp) or Y2H selection conditions: (-Leu/Trp/His + 1 mM $CuSO_4$) without (low stringency) or with 1 mM 3-AT (high stringency). The non-toxic DB-antagonist effector is mated with AD empty vector to screen for autoactivation, the ability to drive *GAL1::HIS3* expression by itself. Plates were incubated for 3 days at 30˚C before imaging.

Figure 2: Performance of the iBFG-Y2H *L. pneumophila* effector screen

A Interaction score matrix of all human positive reference set (hPRS) ORFs. The 21 expected interaction pairs are highlighted in red. The interaction score heatmap is visualized using two ranges, 0-1000 and 1000-31,000, to capture the entire score range.

B Mathew's correlation coefficient (MCC, black), precision (prec, green) and recall (RC, purple) plot for the hPRS. The optimal MCC is indicated with a grey line. The interaction score, precision and recall values at the optimal MCC are listed.

C Bar graph showing the ranked interaction scores of the top 140 interaction pairs above the MCC-optimal threshold. The panels below show the location of the human PRS (blue) and the results of the iBFG-Y2H retest experiment (white - not tested, grey – negative and black – positive). To confirm interaction pairs, ORFs were recloned in inducible AD or DB vectors using confirmed Gateway Entry vectors and transformed to the BFG-Y2H yeast strains. Haploid strains carrying the AD or DB vectors were mated and resulting diploids selected, spotted on control (-Leu/Trp) and Y2H selective (-Leu/Trp/His + 1 mM $CuSO_4$) conditions and grown for 3

days at 30°C. The images of the retest set are shown in Fig EV2, and the results are listed in Table EV4.

Figure 3: Validation of the iBFG-Y2H interaction pairs by the orthologous yN2H method

A The log-transformed normalized luminescence ratio (NLR) from the yN2H experiment is plotted for a random sampling of the human PRS (hsPRS-v2), RRS (hsRRS-v2) and 33 iBFG-Y2H pairs that confirmed in the iBFG-Y2H assay (lpPPIs). The dashed line indicates Log2 NLR value of 1.776 where the Z-score for the RRS is 2.23. Confidence clouds represent a 68.3% Bayesian confidence interval.

B The detection rate of the lpPPI, hsPRS-V2 and hsRRS-V2 based on the threshold in **A**. Error bars represent a 68.3% Bayesian confidence interval. The detection rate of the *L. pneumophila* pairs exceeds the detection rate of the hsPRS-V2 pairs, suggesting robustness of this interaction set.

Figure 4: iBFG-Y2H captures several interactions of the Dot/Icm complex

A The Dot/Icm T4SS interaction score matrix showing the 27 DB- or 28 AD-fusions of the Dot/Icm components present in the screen. The nine interaction pairs that were positive in the iBFG-Y2H retest assay are circled in black, published interactions are indicated with a star.

B Inducible Y2H assay for nine confirmed Dot/Icm-Dot/Icm interaction pairs. ORFs were recloned in unbarcoded, inducible AD or DB vectors using verified Gateway Entry vectors and transformed to the BFG-Y2H yeast strains. Haploid strains carrying the AD or DB vectors were mated and resulting diploids selected and grown as described in Fig 1. To assay for autoactivator activity of the AD or DB fusion, each AD or DB fusion is mated with DB or AD empty vector,

respectively. DB-IcmS is an autoactivator (the ability to grow on -Leu/Trp/His + $CuSO_4$ in the absence of an DB-AD complex), but in the higher stringency conditions (-Leu/Trp/His + $CuSO_4$/3-AT) the DB-IcmS – AD-IcmW diploid can still grow, but DB-IcmS with AD-empty vector diploid cannot.

C Inducible Y2H assay of confirmed effector-Dot/Icm interaction pairs as described above. The core effector RavC, conserved across *Legionella* species, is indicated with a star.

Figure 5: iBFG-Y2H effector-effector protein interactions

A Inducible Y2H assay of confirmed interactions of effectors and putative effectors that self-interact. DB-Lpg2860 is an autoactivator in the low stringency condition (-Leu/Trp/His) but not in the higher stringency condition (-Leu/Trp/His+3-AT) in A and B.

B Inducible Y2H assay of confirmed interactions that involve two effectors or putative effectors. Core effectors conserved in all *Legionella* species are indicated with a star.

Figure 6: iBFG-Y2H interactions of human PRS proteins with effectors and putative effectors

A Inducible Y2H assay of confirmed interactions of effectors and putative effector Lpg2266 with human transcription factor IKZF1. Core effector LegA3 (indicated with a star) is an autoactivator on low stringency medium (-Leu/Trp/His), but not in the higher stringency condition (-Leu/Trp/His+3AT).

B Inducible Y2H assay of confirmed interactions between effectors and several proteins from the human PRS set.

Figure 7: A network view of the iBFG-Y2H interaction pairs

A network showing all the confirmed interaction pairs captures in the iBFG-Y2H screen involving effectors or putative effectors. Effectors are shown as a rectangle, Dot/Icm components as a diamond and human PRS proteins as an oval. Arrows point from DB to AD, the thickness of the edges is reflective of the iBFG-Y2H interaction score. Core effectors are indicated by a star and nodes of previously published PPIs are shown in blue. The network was created using Cytoscape v3.101 (Shannon *et al*, 2003).

Figure EV1: iBFG-Y2H barcode representation and correlation of fusion barcode tags

A, B The bar graphs show the distribution of barcode representation of ORFs in the AD (**A**) and DB (**B**) collection. The majority of ORFs are represented by at least three uniquely barcoded vectors.

C, D Barcode recombination leads to an equal number of up and down fusion barcodes for each unique pair. The scatter plots show the counts of the up-tag fusion barcodes plotted against the down-tag fusion barcodes and the Pearson correlation (PCC) of the barcode pair abundance across the entire population in the control (**C**) and Y2H selective (**D**) conditions. The up- and down-tag fusions show good concordance, which indicates that there is no major barcode-specific effects due to PCR or sequencing.

Figure EV2: Retest of iBFG-Y2H interactions with *L. pneumophila* effectors

All 107 interaction pairs above the MCC optimal threshold involving effectors (effector-effector, effector-human, effector-dot/icm) and Dot/Icm-Dot/Icm pairs were retested. The vectors were recloned from confirmed Gateway entry clones, transformed to BFG-Y2H strains RY1010 and

RY1030 and arrayed in an AD and DB array. A1 in plate 1 and 2 are empty vector controls, see Table EV4 for the ORF identities in each spot.

A The DB array was mated with AD-EV, spotted on control (-Leu/Trp medium) and Y2H selective conditions (-Leu/Trp/His + 1 mM $CuSO_4$) and grown for 3 days before imaging. Two effectors, DB-Lpg2860 and DB-Lpg2300/LegA3, are autoactivators and can grow on Y2H selective conditions in the presence of the AD empty vector.

B The AD array was mated with DB-EV and grown as above.

C The DB array was mated with the AD-array and grown as above. Of the 107 interaction pairs, 56 interactions confirm in the retest experiment.

References

Bastidas RJ, Kędzior M, Davidson RK, Walsh SC, Dolat L, Sixt BS, Pruneda JN, Coers J & Valdivia RH (2024) The acetylase activity of Cdu1 regulates bacterial exit from infected cells by protecting Chlamydia effectors from degradation. *eLife* 12

Belyi Y, Tartakovskaya D, Tais A, Fitzke E, Tzivelekidis T, Jank T, Rospert S & Aktories K (2012) Elongation Factor 1A Is the Target of Growth Inhibition in Yeast Caused by Legionella pneumophila Glucosyltransferase Lgt1. *J Biol Chem* 287: 26029–26037

Bhogaraju S, Bonn F, Mukherjee R, Adams M, Pfleiderer MM, Galej WP, Matkovic V, Lopez-Mosqueda J, Kalayil S, Shin D, *et al* (2019) Inhibition of bacterial ubiquitin ligases by SidJ–calmodulin catalysed glutamylation. *Nature* 572: 382–386

Black MH, Osinski A, Gradowski M, Servage KA, Pawłowski K, Tomchick DR & Tagliabracci VS (2019) Bacterial pseudokinase catalyzes protein polyglutamylation to inhibit the SidE-family ubiquitin ligases. *Science* 364: 787–792

Boamah DK, Zhou G, Ensminger AW & O'Connor TJ (2017) From Many Hosts, One Accidental Pathogen: The Diverse Protozoan Hosts of Legionella. *Front Cell Infect Mi* 7: 477

Brachmann CB, Davies A, Cost GJ, Caputo E, Li J, Hieter P & Boeke JD (1998) Designer deletion strains derived from Saccharomyces cerevisiae S288C: A useful set of strains and plasmids for PCR□mediated gene disruption and other applications. *Yeast* 14: 115–132

Braun P, Tasan M, Dreze M, Barrios-Rodiles M, Lemmens I, Yu H, Sahalie JM, Murray RR, Roncari L, Smet A-S de, *et al* (2009) An experimentally derived confidence score for binary protein-protein interactions. *Nat Methods* 6: 91–97

Bugalhão JN, Mota LJ & Franco IS (2016) Identification of regions within the Legionella pneumophila VipA effector protein involved in actin binding and polymerization and in interference with eukaryotic organelle trafficking. *Microbiologyopen* 5: 118–133

Burstein D, Amaro F, Zusman T, Lifshitz Z, Cohen O, Gilbert JA, Pupko T, Shuman HA & Segal G (2016) Genomic analysis of 38 Legionella species identifies large and diverse effector repertoires. *Nat Genet* 48: 167–175

Burstein D, Zusman T, Degtyar E, Viner R, Segal G & Pupko T (2009) Genome-Scale Identification of Legionella pneumophila Effectors Using a Machine Learning Approach. *Plos Pathog* 5: e1000508

Butt TR & Ecker DJ (1987) Yeast metallothionein and applications in biotechnology. *Microbiol Rev* 51: 351–64

Camacho C, Coulouris G, Avagyan V, Ma N, Papadopoulos J, Bealer K & Madden TL (2009) BLAST+: architecture and applications. *BMC Bioinform* 10: 421

Campodonico EM, Chesnel L & Roy CR (2005) A yeast genetic system for the identification and characterization of substrate proteins transferred into host cells by the Legionella pneumophila Dot/Icm system. *Mol Microbiol* 56: 918–933

Choi SG, Olivet J, Cassonnet P, Vidalain P-O, Luck K, Lambourne L, Spirohn K, Lemmens I, Santos MD, Demeret C, *et al* (2019) Maximizing binary interactome mapping with a minimal number of assays. *Nat Commun* 10: 3907

Chua MD, Mineva GM & Guttman JA (2023) Ube2N is present and functions within listeria Actin□rich structures and lamellipodia: A localization and pharmacological inhibition study. *Anat Rec* 306: 1140–1148

Chua MD, Moon K, Foster LJ & Guttman JA (2018) Whole cell and bacterial movement: The identification of the ubiquitin E2 enzyme (Ube2N) as a novel actin□associated protein. *FASEB J* 32: 369.4-369.4

Coers J, Kagan JC, Matthews M, Nagai H, Zuckman DM & Roy CR (2000) Identification of Icm protein complexes that play distinct roles in the biogenesis of an organelle permissive for Legionella pneumophila intracellular growth. *Mol Microbiol* 38: 719–736

Dean P, Mühlen S, Quitard S & Kenny B (2010) The bacterial effectors EspG and EspG2 induce a destructive calpain activity that is kept in check by the co□delivered Tir effector. *Cell Microbiol* 12: 1308–1321

de Felipe KS, Glover RT, Charpentier X, Anderson OR, Reyes M, Pericone CD & Shuman HA (2008) Legionella Eukaryotic-Like Type IV Substrates Interfere with Organelle Trafficking. *PLoS Pathog* 4: e1000117

Dong N, Niu M, Hu L, Yao Q, Zhou R & Shao F (2016) Modulation of membrane phosphoinositide dynamics by the phosphatidylinositide 4-kinase activity of the Legionella LepB effector. *Nat Microbiol* 2: 16236

Duménil G & Isberg RR (2001) The Legionella pneumophila IcmR protein exhibits chaperone activity for IcmQ by preventing its participation in high□molecular□weight complexes. *Mol Microbiol* 40: 1113–1127

Durie CL, Sheedlo MJ, Chung JM, Byrne BG, Su M, Knight T, Swanson M, Lacy DB & Ohi MD (2020) Structural analysis of the Legionella pneumophila Dot/Icm type IV secretion system core complex. *eLife* 9: e59530

Ensminger AW (2016) Legionella pneumophila, armed to the hilt: justifying the largest arsenal of effectors in the bacterial world. *Curr Opin Microbiol* 29: 74–80

Faulkner G, Berk SG, Garduño E, Ortiz-Jiménez MA & Garduño RA (2008) Passage through Tetrahymena tropicalis Triggers a Rapid Morphological Differentiation in Legionella pneumophila. *J Bacteriol* 190: 7728–7738

Fields BS (1996) The molecular ecology of legionellae. *Trends Microbiol* 4: 286–290

Fields BS, Benson RF & Besser RE (2002) Legionella and Legionnaires' Disease: 25 Years of Investigation. *Clin Microbiol Rev* 15: 506–526

Fields S & Song O (1989) A novel genetic system to detect protein–protein interactions. *Nature* 340: 245–246

Finsel I & Hilbi H (2015) Formation of a pathogen vacuole according to Legionella pneumophila: how to kill one bird with many stones. *Cell Microbiol* 17: 935–950

Franco IS, Shohdy N & Shuman HA (2012) The Legionella pneumophila Effector VipA Is an Actin Nucleator That Alters Host Cell Organelle Trafficking. *Plos Pathog* 8: e1002546

Gan N, Guan H, Huang Y, Yu T, Fu J, Nakayasu ES, Puvar K, Das C, Wang D, Ouyang S, *et al* (2020) Legionella pneumophila regulates the activity of UBE2N by deamidase□mediated deubiquitination. *Embo J* 39: e102806

Gan N, Nakayasu ES, Hollenbeck PJ & Luo Z-Q (2019a) Legionella pneumophila inhibits immune signalling via MavC-mediated transglutaminase-induced ubiquitination of UBE2N. *Nat Microbiol* 4: 134–143

Gan N, Zhen X, Liu Y, Xu X, He C, Qiu J, Liu Y, Fujimoto GM, Nakayasu ES, Zhou B, *et al* (2019b) Regulation of phosphoribosyl ubiquitination by a calmodulin-dependent glutamylase. *Nature* 572: 387–391

Ge J, Xu H, Li T, Zhou Y, Zhang Z, Li S, Liu L & Shao F (2009) A Legionella type IV effector activates the NF-κB pathway by phosphorylating the IκB family of inhibitors. *Proc National Acad Sci* 106: 13725–13730

Ghosal D, Jeong KC, Chang Y-W, Gyore J, Teng L, Gardner A, Vogel JP & Jensen GJ (2019) Molecular architecture, polar targeting and biogenesis of the Legionella Dot/Icm T4SS. *Nat Microbiol* 4: 1173–1182

Gietz RD & Schiestl RH (2007a) Frozen competent yeast cells that can be transformed with high efficiency using the LiAc/SS carrier DNA/PEG method. *Nat Protoc* 2: 1–4

Gietz RD & Schiestl RH (2007b) High-efficiency yeast transformation using the LiAc/SS carrier DNA/PEG method. *Nat Protoc* 2: 31–34

Gomez-Valero L, Rusniok C, Carson D, Mondino S, Pérez-Cobas AE, Rolando M, Pasricha S, Reuter S, Demirtas J, Crumbach J, *et al* (2019) More than 18,000 effectors in the Legionella

genus genome provide multiple, independent combinations for replication in human cells. *Proc National Acad Sci* 116: 201808016

Guo Z, Stephenson R, Qiu J, Zheng S & Luo Z-Q (2014) A Legionella effector modulates host cytoskeletal structure by inhibiting actin polymerization. *Microbes Infect* 16: 225–236

He L, Lin Y, Ge Z, He S, Zhao B, Shen D, He J & Lu Y (2019) The Legionella pneumophila effector WipA disrupts host F□actin polymerisation by hijacking phosphotyrosine signalling. *Cell Microbiol* 21: e13014

Heidtman M, Chen EJ, Moy M & Isberg RR (2009) Large□scale identification of Legionella pneumophila Dot/Icm substrates that modulate host cell vesicle trafficking pathways. *Cell Microbiol* 11: 230–248

Hervet E, Charpentier X, Vianney A, Lazzaroni J-C, Gilbert C, Atlan D & Doublet P (2011) Protein Kinase LegK2 Is a Type IV Secretion System Effector Involved in Endoplasmic Reticulum Recruitment and Intracellular Replication of Legionella pneumophila. *Infect Immun* 79: 1936–1950

Hsieh T-S, Lopez VA, Black MH, Osinski A, Pawłowski K, Tomchick DR, Liou J & Tagliabracci VS (2021) Dynamic remodeling of host membranes by self-organizing bacterial effectors. *Science* 372: 935–941

Huang L, Boyd D, Amyot WM, Hempstead AD, Luo Z, O'Connor TJ, Chen C, Machner M, Montminy T & Isberg RR (2011) The E Block motif is associated with Legionella pneumophila translocated substrates. *Cell Microbiol* 13: 227–245

Isberg RR, O'Connor TJ & Heidtman M (2009) The Legionella pneumophila replication vacuole: making a cosy niche inside host cells. *Nat Rev Microbiol* 7: 13–24

Jeong KC, Sexton JA & Vogel JP (2015) Spatiotemporal Regulation of a Legionella pneumophila T4SS Substrate by the Metaeffector SidJ. *Plos Pathog* 11: e1004695

Jia Q, Lin Y, Gou X, He L, Shen D, Chen D, Xie W & Lu Y (2018) Legionella pneumophila effector WipA, a bacterial PPP protein phosphatase with PTP activity. *Acta Biochim Biophys Sin* 50: 547–554

Joseph AM, Pohl AE, Ball TJ, Abram TG, Johnson DK, Geisbrecht BV & Shames SR (2020) The Legionella pneumophila Metaeffector Lpg2505 (MesI) Regulates SidI-Mediated Translation Inhibition and Novel Glycosyl Hydrolase Activity. *Infect Immun* 88

Joseph AM & Shames SR (2021) Affecting the Effectors: Regulation of Legionella pneumophila Effector Function by Metaeffectors. *Pathogens* 10: 108

Kim H, Kubori T, Yamazaki K, Kwak M-J, Park S-Y, Nagai H, Vogel JP & Oh B-H (2020) Structural basis for effector protein recognition by the Dot/Icm Type IVB coupling protein complex. *Nat Commun* 11: 2623

Kubori T & Galán JE (2003) Temporal Regulation of Salmonella Virulence Effector Function by Proteasome-Dependent Protein Degradation. *Cell* 115: 333–342

Kubori T & Nagai H (2011) Bacterial Effector-Involved Temporal and Spatial Regulation by Hijack of the Host Ubiquitin Pathway. *Front Microbiol* 2: 145

Kubori T, Shinzawa N, Kanuka H & Nagai H (2010) Legionella Metaeffector Exploits Host Proteasome to Temporally Regulate Cognate Effector. *Plos Pathog* 6: e1001216

Kuehn HS, Boast B & Rosenzweig SD (2022) Inborn errors of human IKAROS: LOF and GOF variants associated with primary immunodeficiency. *Clin Exp Immunol* 212: 129–136

Kwak M-J, Kim JD, Kim H, Kim C, Bowman JW, Kim S, Joo K, Lee J, Jin KS, Kim Y-G, *et al* (2017) Architecture of the type IV coupling protein complex of Legionella pneumophila. *Nat Microbiol* 2: 17114

Langmead B & Salzberg SL (2012) Fast gapped-read alignment with Bowtie 2. *Nat Methods* 9: 357–359

Larson CL, Beare PA, Howe D & Heinzen RA (2013) Coxiella burnetii effector protein subverts clathrin-mediated vesicular trafficking for pathogen vacuole biogenesis. *Proc National Acad Sci* 110: E4770–E4779

Lesser CF & Miller SI (2001) Expression of microbial virulence proteins in Saccharomyces cerevisiae models mammalian infection. *EMBO J* 20: 1840–1849

Liu M, Conover GM & Isberg RR (2008) Legionella pneumophila EnhC is required for efficient replication in tumour necrosis factor α□stimulated macrophages. *Cell Microbiol* 10: 1906–1923

Liu Y, Zhu W, Tan Y, Nakayasu ES, Staiger CJ & Luo Z-Q (2017) A Legionella Effector Disrupts Host Cytoskeletal Structure by Cleaving Actin. *PLoS Pathog* 13: e1006186

Losick VP, Haenssler E, Moy M & Isberg RR (2010) LnaB: a Legionella pneumophila activator of NF□κB. *Cell Microbiol* 12: 1083–1097

Luck K, Kim D-K, Lambourne L, Spirohn K, Begg BE, Bian W, Brignall R, Cafarelli T, Campos-Laborie FJ, Charloteaux B, *et al* (2020) A reference map of the human binary protein interactome. *Nature* 580: 402–408

Luo Z-Q & Isberg RR (2004) Multiple substrates of the Legionella pneumophila Dot/Icm system identified by interbacterial protein transfer. *P Natl Acad Sci Usa* 101: 841–846

Magori S & Citovsky V (2011) Agrobacterium Counteracts Host-Induced Degradation of Its Effector F-Box Protein. *Sci Signal* 4: ra69–ra69

McCloskey A, Perri K, Chen T, Han A & Luo Z-Q (2021) The metaeffector MesI regulates the activity of the Legionella effector SidI through direct protein–protein interactions. *Microbes Infect* 23: 104794

Meir A, Chetrit D, Liu L, Roy CR & Waksman G (2018) Legionella DotM structure reveals a role in effector recruiting to the Type 4B secretion system. *Nat Commun* 9: 507

Meir A, Macé K, Lukoyanova N, Chetrit D, Hospenthal MK, Redzej A, Roy C & Waksman G (2020) Mechanism of effector capture and delivery by the type IV secretion system from Legionella pneumophila. *Nat Commun* 11: 2864

Mengue L, Régnacq M, Aucher W, Portier E, Héchard Y & Samba-Louaka A (2016) Legionella pneumophila prevents proliferation of its natural host Acanthamoeba castellanii. *Sci Rep* 6: 36448

Michard C, Sperandio D, Baïlo N, Pizarro-Cerdá J, LeClaire L, Chadeau-Argaud E, Pombo-Grégoire I, Hervet E, Vianney A, Gilbert C, *et al* (2015) The Legionella Kinase LegK2 Targets the ARP2/3 Complex To Inhibit Actin Nucleation on Phagosomes and Allow Bacterial Evasion of the Late Endocytic Pathway. *Mbio* 6: e00354-15

Molmeret M, Horn M, Wagner M, Santic M & Kwaik YA (2005) Amoebae as Training Grounds for Intracellular Bacterial Pathogens. *Appl Environ Microbiol* 71: 20–28

Mount HO, Zangari F, Gingras A-C & Ensminger AW (2022) The L. pneumophila effector PieF modulates mRNA stability through association with eukaryotic CCR4-NOT. *Biorxiv*: 2022.06.06.494580

Mukherjee S, Liu X, Arasaki K, McDonough J, Galán JE & Roy CR (2011) Modulation of Rab GTPase function by a protein phosphocholine transferase. *Nature* 477: 103–106

Müller MP, Peters H, Blümer J, Blankenfeldt W, Goody RS & Itzen A (2010) The *Legionella* Effector Protein DrrA AMPylates the Membrane Traffic Regulator Rab1b. *Science* 329: 946–949

Neunuebel MR, Chen Y, Gaspar AH, Backlund PS, Yergey A & Machner MP (2011) De-AMPylation of the Small GTPase Rab1 by the Pathogen Legionella pneumophila. *Science* 333: 453–456

Nevo O, Zusman T, Rasis M, Lifshitz Z & Segal G (2014) Identification of Legionella pneumophila Effectors Regulated by the LetAS-RsmYZ-CsrA Regulatory Cascade, Many of Which Modulate Vesicular Trafficking. *J Bacteriol* 196: 681–692

Ninio S, Zuckman□Cholon DM, Cambronne ED & Roy CR (2005) The Legionella IcmS–IcmW protein complex is important for Dot/Icm□mediated protein translocation. *Mol Microbiol* 55: 912–926

Oh K-S, Gottschalk RA, Lounsbury NW, Sun J, Dorrington MG, Baek S, Sun G, Wang Z, Krauss KS, Milner JD, *et al* (2018) Dual Roles for Ikaros in Regulation of Macrophage Chromatin State and Inflammatory Gene Expression. *J Immunol* 201: 757–771

Pinotsis N & Waksman G (2017) Structure of the WipA protein reveals a novel tyrosine protein phosphatase effector from Legionella pneumophila. *J Biol Chem* 292: 9240–9251

Pollock TY, Marrero VRV, Brodsky IE & Shin S (2023) TNF licenses macrophages to undergo rapid caspase-1, -11, and -8-mediated cell death that restricts Legionella pneumophila infection. *PLOS Pathog* 19: e1010767

Rao C, Benhabib H & Ensminger AW (2013) Phylogenetic Reconstruction of the Legionella pneumophila Philadelphia-1 Laboratory Strains through Comparative Genomics. *Plos One* 8: e64129

Rolland T, Taşan M, Charloteaux B, Pevzner SJ, Zhong Q, Sahni N, Yi S, Lemmens I, Fontanillo C, Mosca R, *et al* (2014) A Proteome-Scale Map of the Human Interactome Network. *Cell* 159: 1212–1226

Rowbotham TJ (1980) Preliminary report on the pathogenicity of Legionella pneumophila for freshwater and soil amoebae. *J Clin Pathol* 33: 1179

Rual J-F, Venkatesan K, Hao T, Hirozane-Kishikawa T, Dricot A, Li N, Berriz GF, Gibbons FD, Dreze M, Ayivi-Guedehoussou N, *et al* (2005) Towards a proteome-scale map of the human protein–protein interaction network. *Nature* 437: 1173–1178

Schator D, Mondino S, Berthelet J, Silvestre CD, Assaya MB, Rusniok C, Rodrigues-Lima F, Wehenkel A, Buchrieser C & Rolando M (2023) Legionella para-effectors target chromatin and promote bacterial replication. *Nat Commun* 14: 2154

Sexton JA, Pinkner JS, Roth R, Heuser JE, Hultgren SJ & Vogel JP (2004) The Legionella pneumophila PilT Homologue DotB Exhibits ATPase Activity That Is Critical for Intracellular Growth. *J Bacteriol* 186: 1658–1666

Shames SR & Finlay BB (2012) Bacterial effector interplay: a new way to view effector function. *Trends Microbiol* 20: 214–219

Shames SR, Liu L, Havey JC, Schofield WB, Goodman AL & Roy CR (2017) Multiple Legionella pneumophila effector virulence phenotypes revealed through high-throughput analysis of targeted mutant libraries. *Proc National Acad Sci* 114: E10446–E10454

Shannon P, Markiel A, Ozier O, Baliga NS, Wang JT, Ramage D, Amin N, Schwikowski B & Ideker T (2003) Cytoscape: A Software Environment for Integrated Models of Biomolecular Interaction Networks. *Genome Res* 13: 2498–2504

Shi X, Halder P, Yavuz H, Jahn R & Shuman HA (2016) Direct targeting of membrane fusion by SNARE mimicry: Convergent evolution of Legionella effectors. *Proc National Acad Sci* 113: 8807–8812

Shohdy N, Efe JA, Emr SD & Shuman HA (2005) Pathogen effector protein screening in yeast identifies Legionella factors that interfere with membrane trafficking. *P Natl Acad Sci Usa* 102: 4866–4871

Siddiqui R, Makhlouf Z & Khan NA (2021) The increasing importance of Vermamoeba vermiformis. *J Eukaryot Microbiol* 68: e12857

Simonis N, Rual J-F, Carvunis A-R, Tasan M, Lemmens I, Hirozane-Kishikawa T, Hao T, Sahalie JM, Venkatesan K, Gebreab F, *et al* (2009) Empirically controlled mapping of the Caenorhabditis elegans protein-protein interactome network. *Nat Methods* 6: 47–54

Sol A, Lipo E, Jesús-Díaz DA de, Murphy C, Devereux M & Isberg RR (2019) Legionella pneumophila translocated translation inhibitors are required for bacterial-induced host cell cycle arrest. *Proc National Acad Sci* 116: 201820093

Song L, Xie Y, Li C, Wang L, He C, Zhang Y, Yuan J, Luo J, Liu X, Xiu Y, *et al* (2021) The Legionella Effector SdjA Is a Bifunctional Enzyme That Distinctly Regulates Phosphoribosyl Ubiquitination. *Mbio* 12: e02316-21

Sutherland MC, Binder KA, Cualing PY & Vogel JP (2013) Reassessing the Role of DotF in the Legionella pneumophila Type IV Secretion System. *Plos One* 8: e65529

Sutherland MC, Nguyen TL, Tseng V & Vogel JP (2012) The Legionella IcmSW Complex Directly Interacts with DotL to Mediate Translocation of Adaptor-Dependent Substrates. *Plos Pathog* 8: e1002910

Tan Y, Arnold RJ & Luo Z-Q (2011) Legionella pneumophila regulates the small GTPase Rab1 activity by reversible phosphorylcholination. *Proc National Acad Sci* 108: 21212–21217

Tan Y & Luo Z-Q (2011) Legionella pneumophila SidD is a deAMPylase that modifies Rab1. *Nature* 475: 506–509

Urbanus ML, Quaile AT, Stogios PJ, Morar M, Rao C, Leo RD, Evdokimova E, Lam M, Oatway C, Cuff ME, *et al* (2016) Diverse mechanisms of metaeffector activity in an intracellular bacterial pathogen, Legionella pneumophila. *Mol Syst Biol* 12: 893

Valleau D, Quaile AT, Cui H, Xu X, Evdokimova E, Chang C, Cuff ME, Urbanus ML, Houliston S, Arrowsmith CH, *et al* (2018) Discovery of Ubiquitin Deamidases in the Pathogenic Arsenal of Legionella pneumophila. *Cell Reports* 23: 568–583

Venkatesan K, Rual J-F, Vazquez A, Stelzl U, Lemmens I, Hirozane-Kishikawa T, Hao T, Zenkner M, Xin X, Goh K-I, *et al* (2009) An empirical framework for binary interactome mapping. *Nat Methods* 6: 83–90

Vincent CD, Friedman JR, Jeong KC, Buford EC, Miller JL & Vogel JP (2006) Identification of the core transmembrane complex of the Legionella Dot/Icm type IV secretion system. *Mol Microbiol* 62: 1278–1291

Vincent CD, Friedman JR, Jeong KC, Sutherland MC & Vogel JP (2012) Identification of the DotL coupling protein subcomplex of the Legionella Dot/Icm type IV secretion system. *Mol Microbiol* 85: 378–391

Vincent CD & Vogel JP (2006) The Legionella pneumophila IcmS–LvgA protein complex is important for Dot/Icm□dependent intracellular growth. *Mol Microbiol* 61: 596–613

Wan M, Sulpizio AG, Akturk A, Beck WHJ, Lanz M, Faça VM, Smolka MB, Vogel JP & Mao Y (2019) Deubiquitination of phosphoribosyl-ubiquitin conjugates by phosphodiesterase-domain–containing Legionella effectors. *Proc National Acad Sci* 116: 23518–23526

Wang Y, Zhan Q, Wang X, Li P, Liu S, Gao G & Gao P (2020) Insights into catalysis and regulation of non-canonical ubiquitination and deubiquitination by bacterial deamidase effectors. *Nat Commun* 11: 2751

Watanabe K, Nakao R, Fujishima M, Tachibana M, Shimizu T & Watarai M (2016) Ciliate Paramecium is a natural reservoir of Legionella pneumophila. *Sci Rep* 6: 24322

Xu J, Xu D, Wan M, Yin L, Wang X, Wu L, Liu Y, Liu X, Zhou Y & Zhu Y (2017) Structural insights into the roles of the IcmS–IcmW complex in the type IVb secretion system of Legionella pneumophila. *Proc National Acad Sci* 114: 13543–13548

Xu L, Shen X, Bryan A, Banga S, Swanson MS & Luo Z-Q (2010) Inhibition of Host Vacuolar H+-ATPase Activity by a Legionella pneumophila Effector. *PLoS Pathog* 6: e1000822

Yachie N, Petsalaki E, Mellor JC, Weile J, Jacob Y, Verby M, Ozturk SB, Li S, Cote AG, Mosca R, *et al* (2016) Pooled□matrix protein interaction screens using Barcode Fusion Genetics. *Mol Syst Biol* 12: 863

Yu H, Braun P, Yıldırım MA, Lemmens I, Venkatesan K, Sahalie J, Hirozane-Kishikawa T, Gebreab F, Li N, Simonis N, *et al* (2008) High-Quality Binary Protein Interaction Map of the Yeast Interactome Network. *Science* 322: 104–110

Zhang T, Lei J, Yang H, Xu K, Wang R & Zhang Z (2011) An improved method for whole protein extraction from yeast Saccharomyces cerevisiae. *Yeast* 28: 795–798

Zhu W, Banga S, Tan Y, Zheng C, Stephenson R, Gately J & Luo Z-Q (2011) Comprehensive Identification of Protein Substrates of the Dot/Icm Type IV Transporter of Legionella pneumophila. *Plos One* 6: e17638

Figure 1 - inducible BFG-Y2H

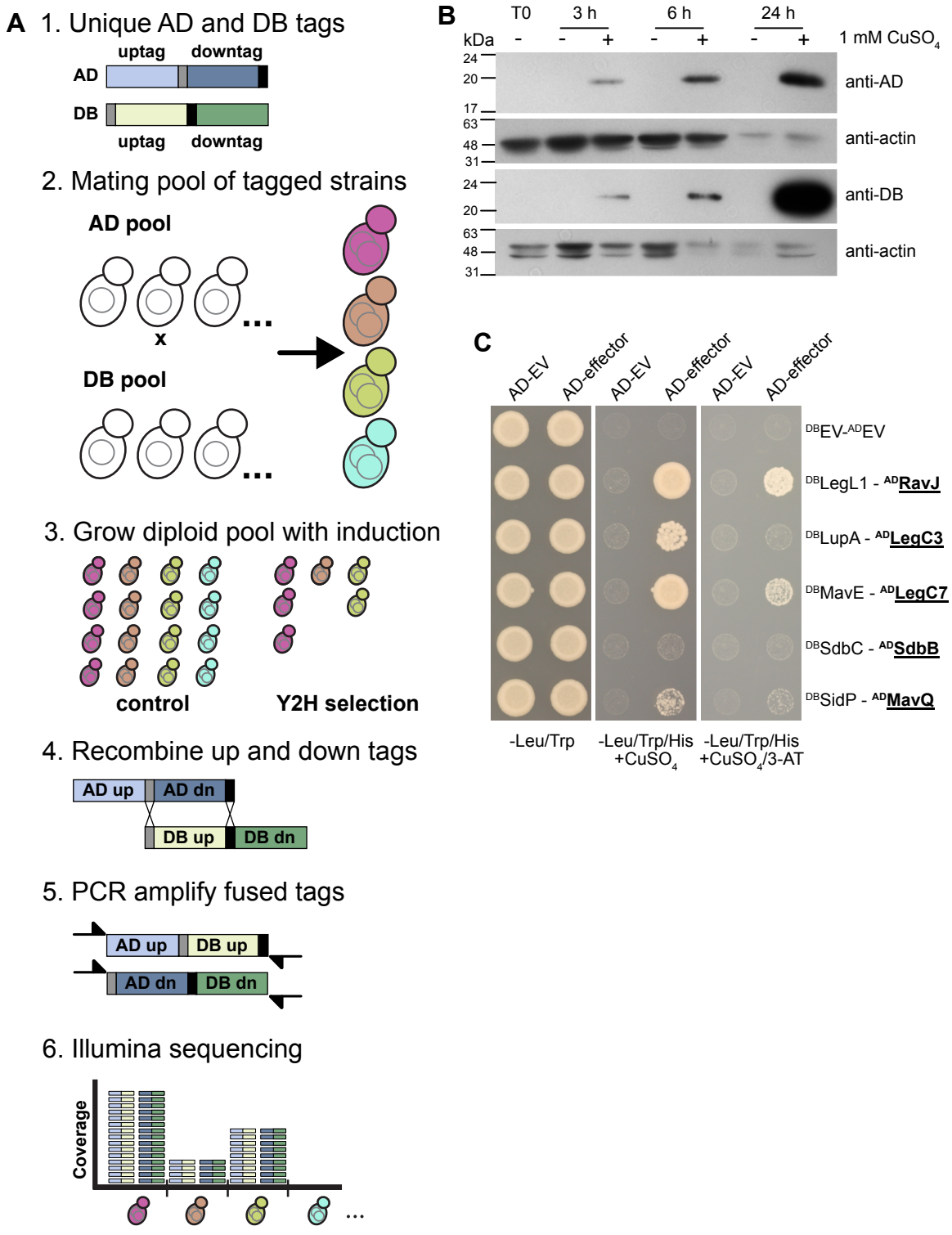

Figure 2 - Performance of the inducible BFG-Y2H *L. pneumophila* effector screen

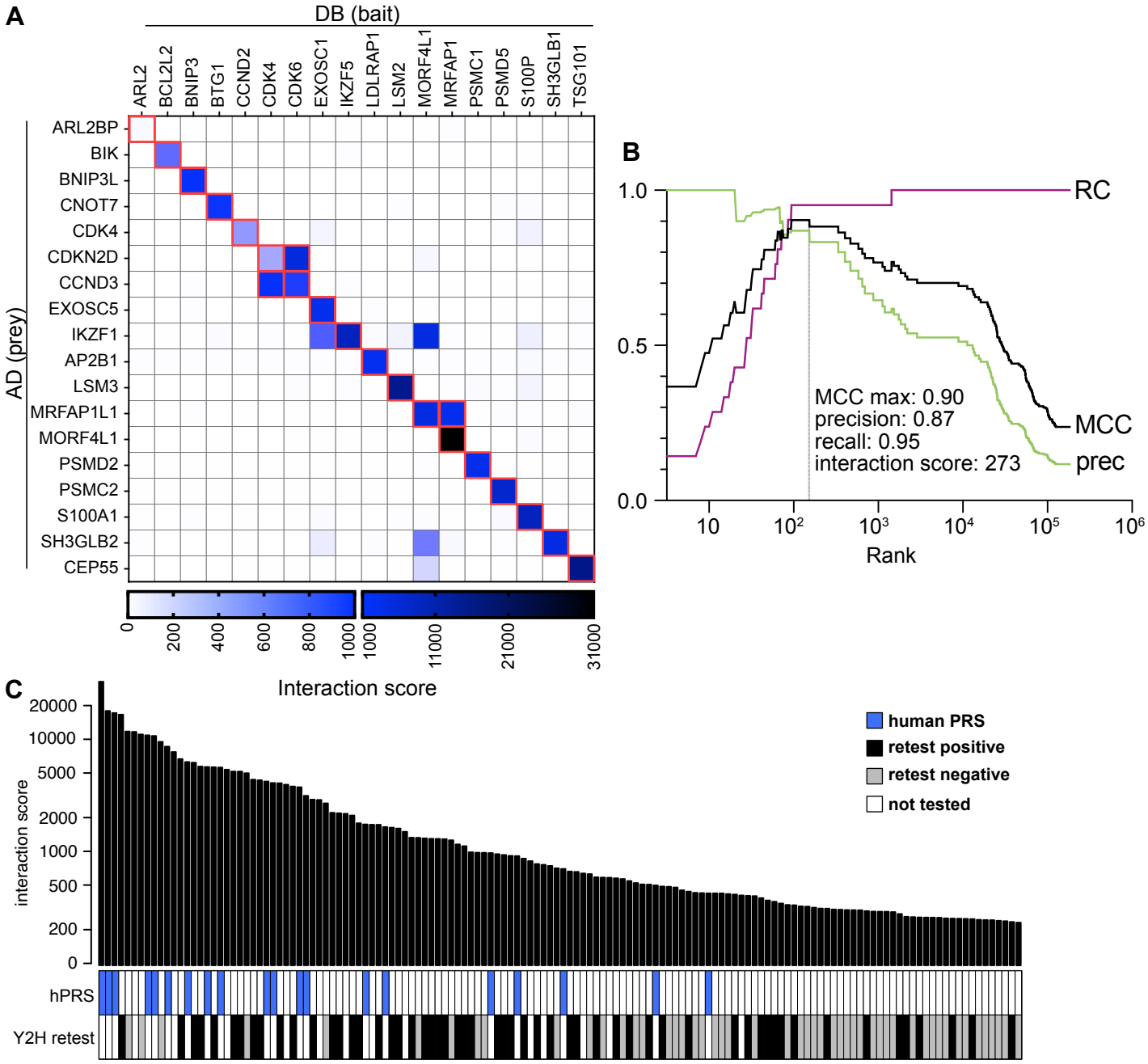

Figure 3 - Validation of the iBFG-Y2H interaction pairs by the orthologous yN2H method

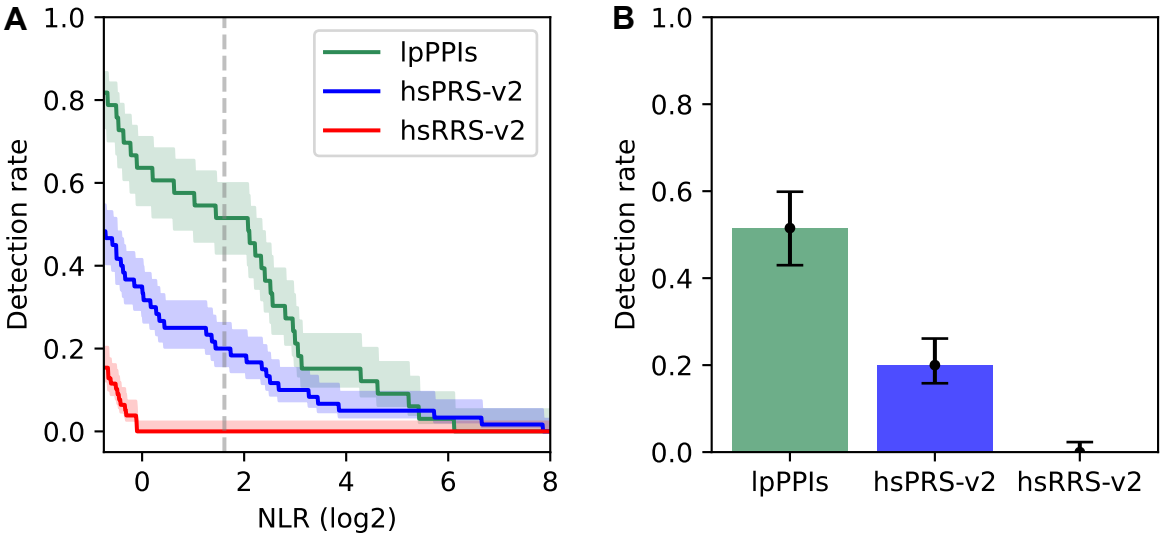

Figure 4 iBFG-Y2H captures several interactions of the Dot/Icm complex

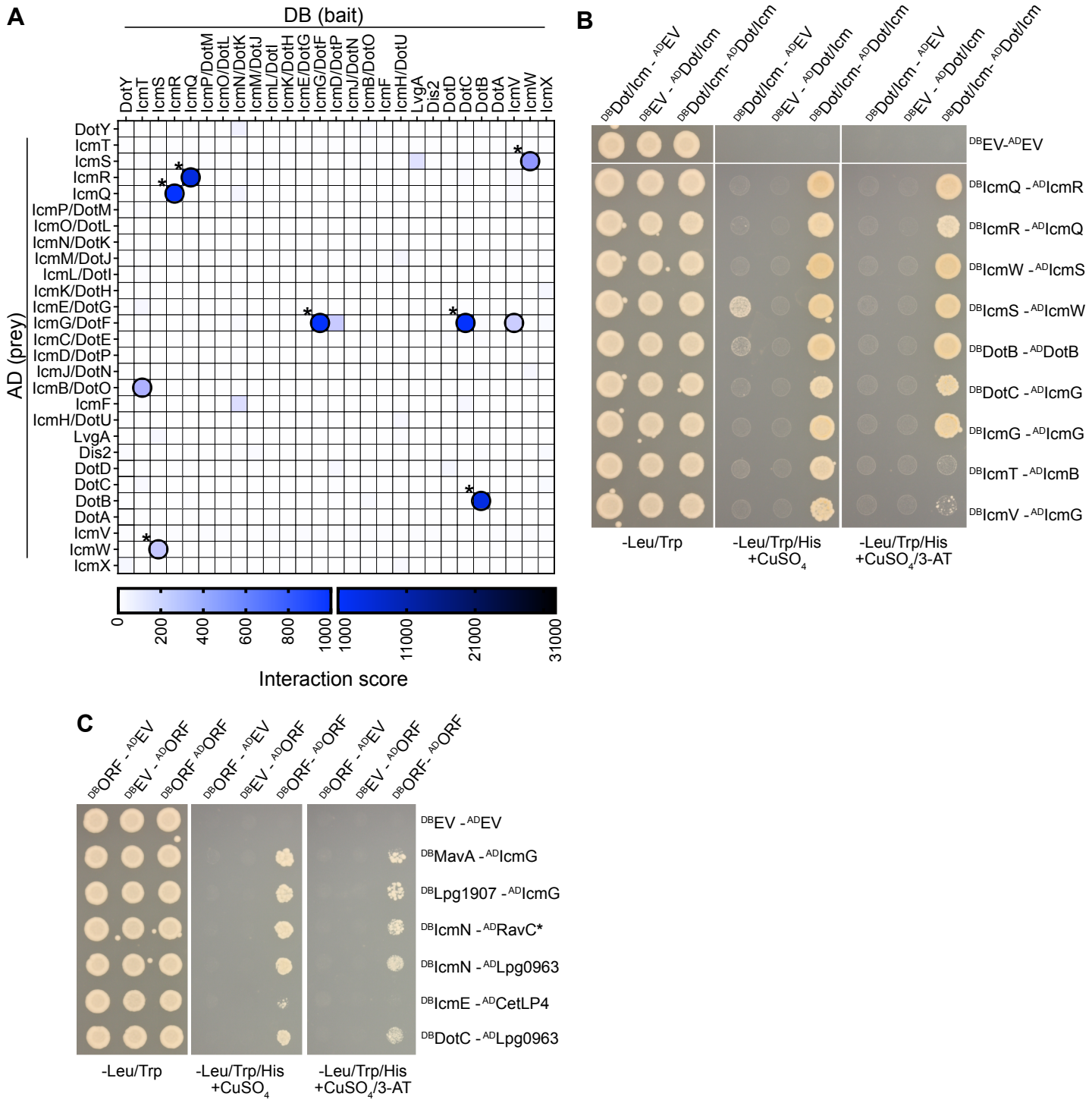

Figure 5 - iBFG-Y2H effector-effector interaction pairs

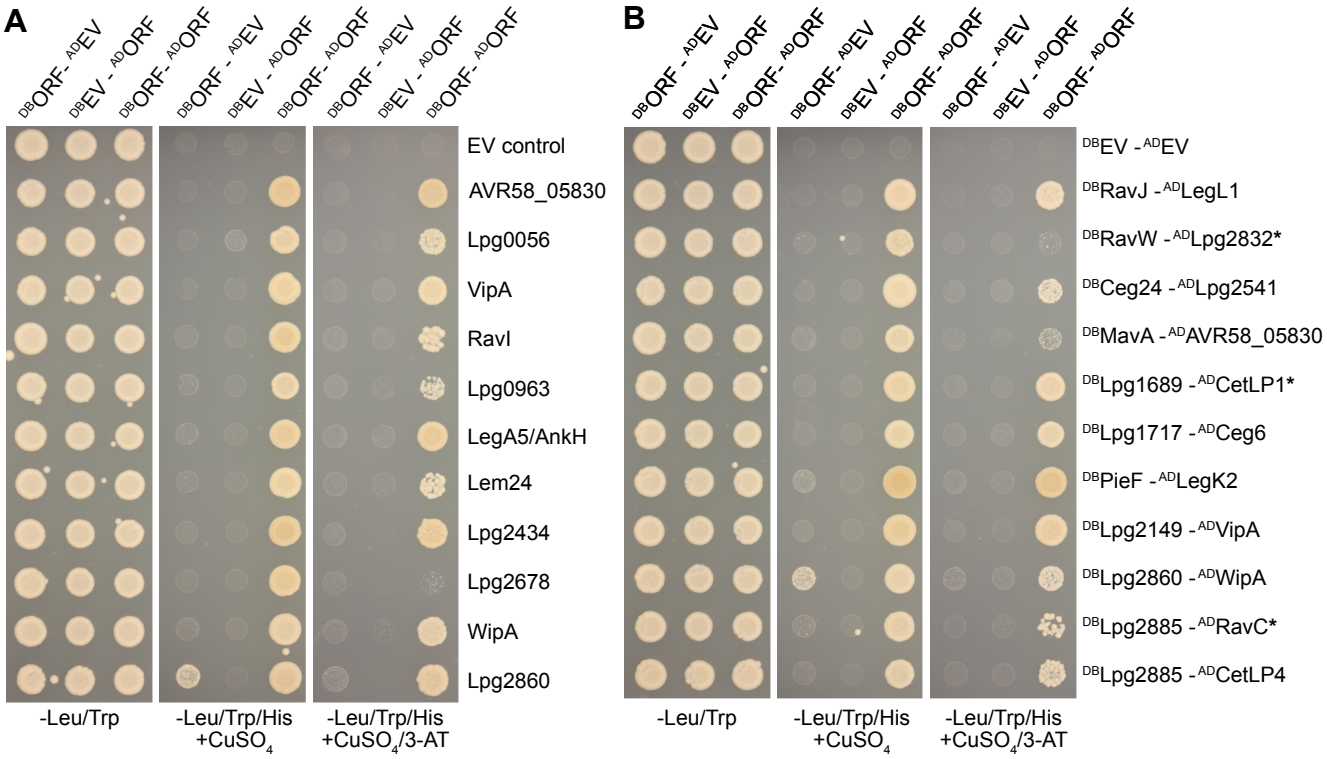

Figure 6 - iBFG-Y2H interactions of human PRS proteins with effectors and putative effectors

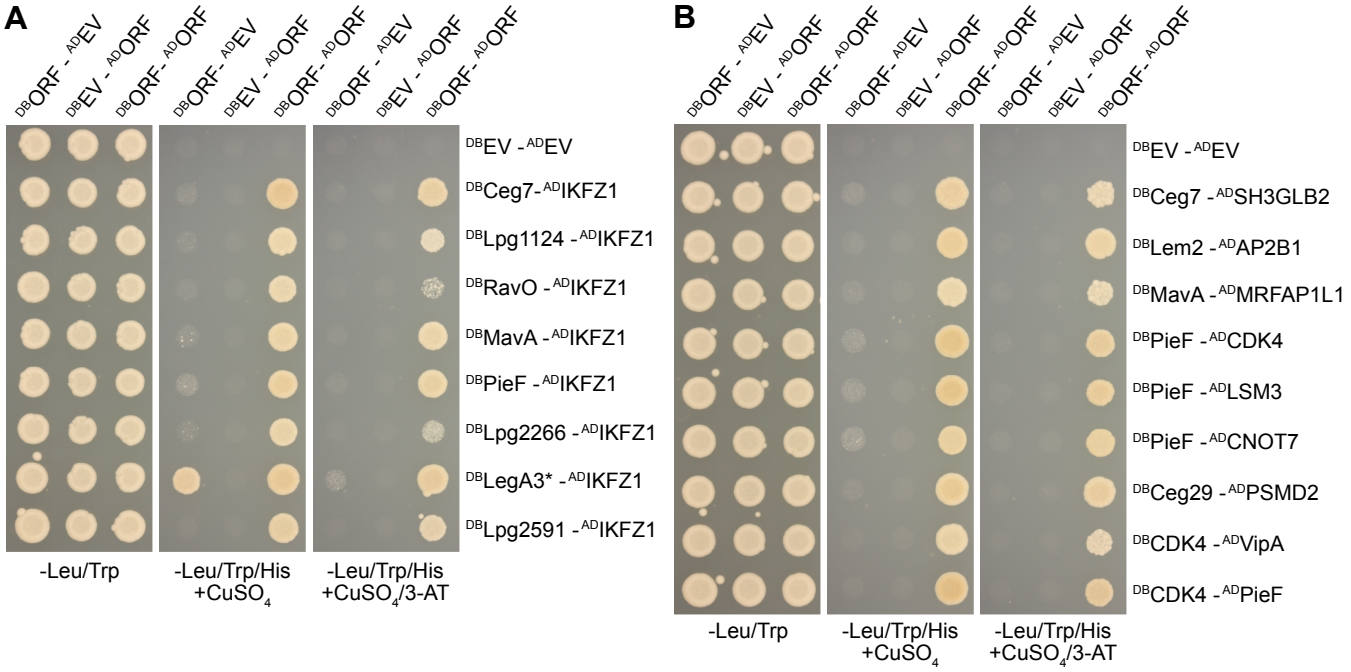

Figure 7 - A network view of the effector interaction pairs

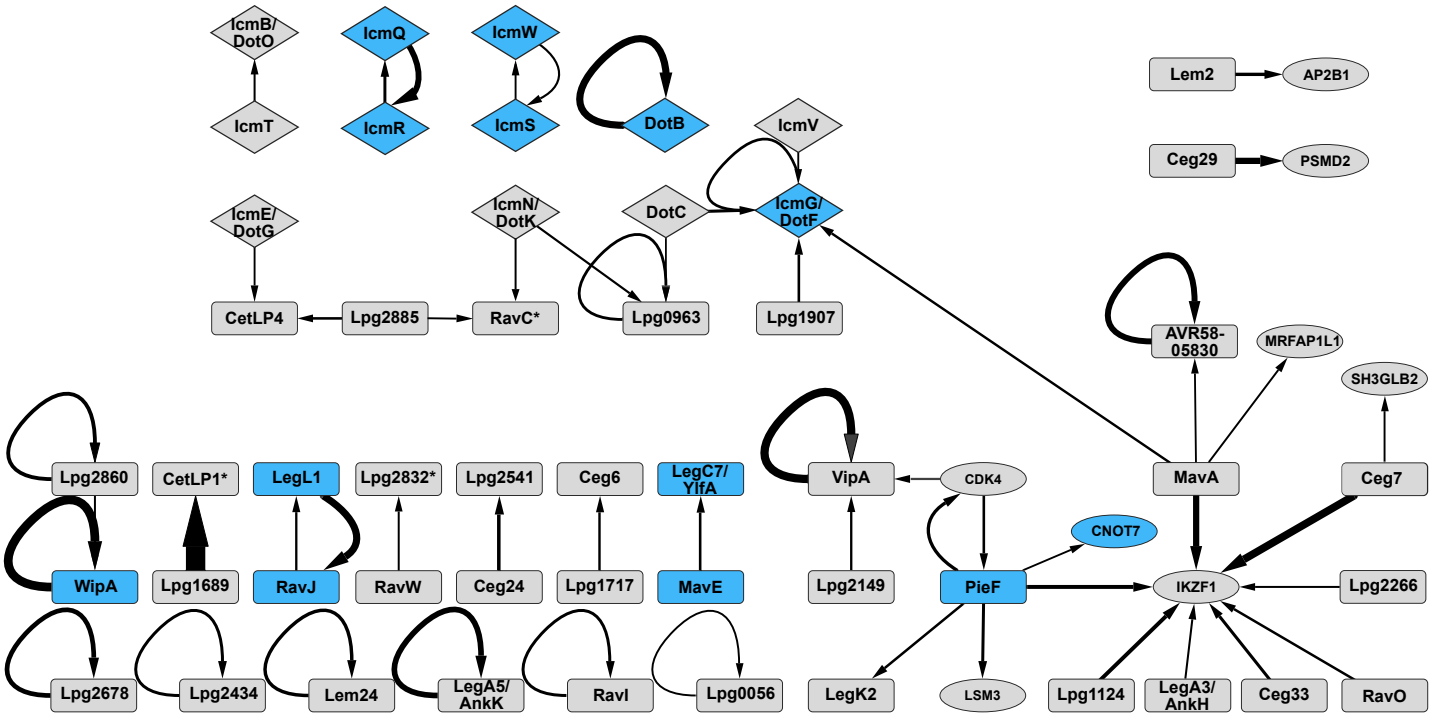

Figure EV1 - iBFG-Y2H barcode representation and correlation of fusion barcode tags

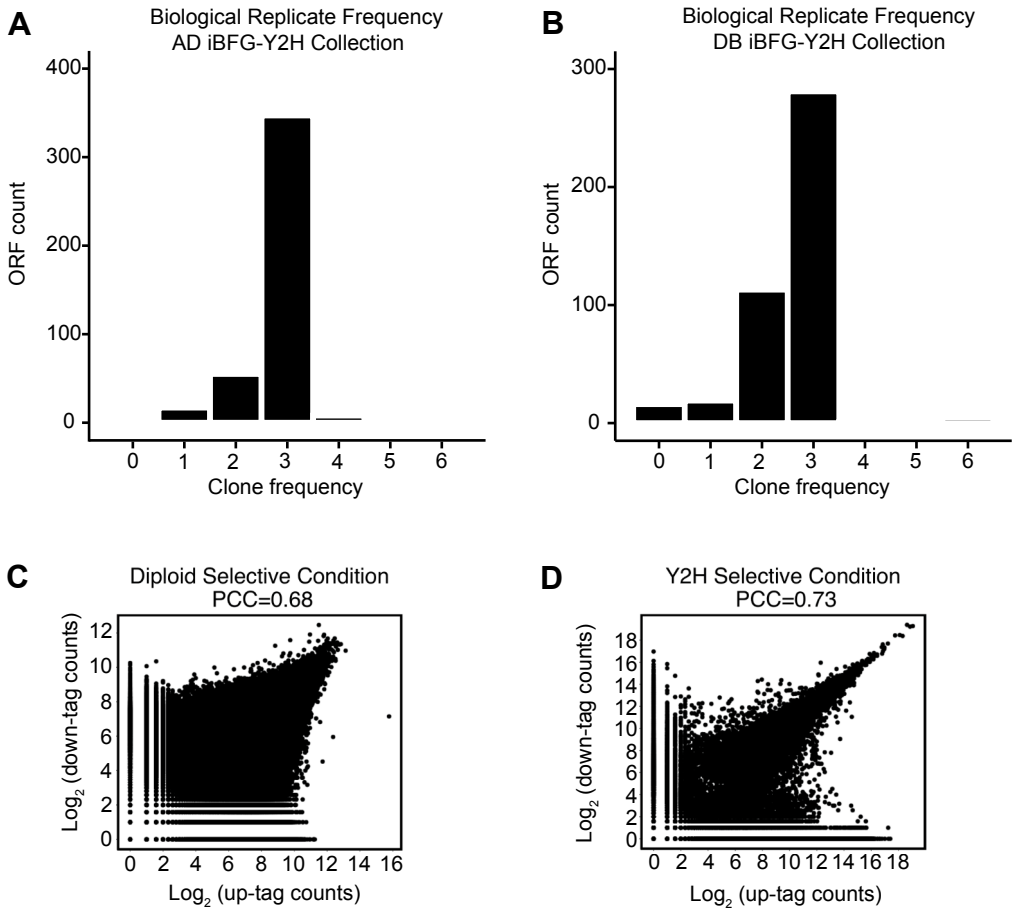
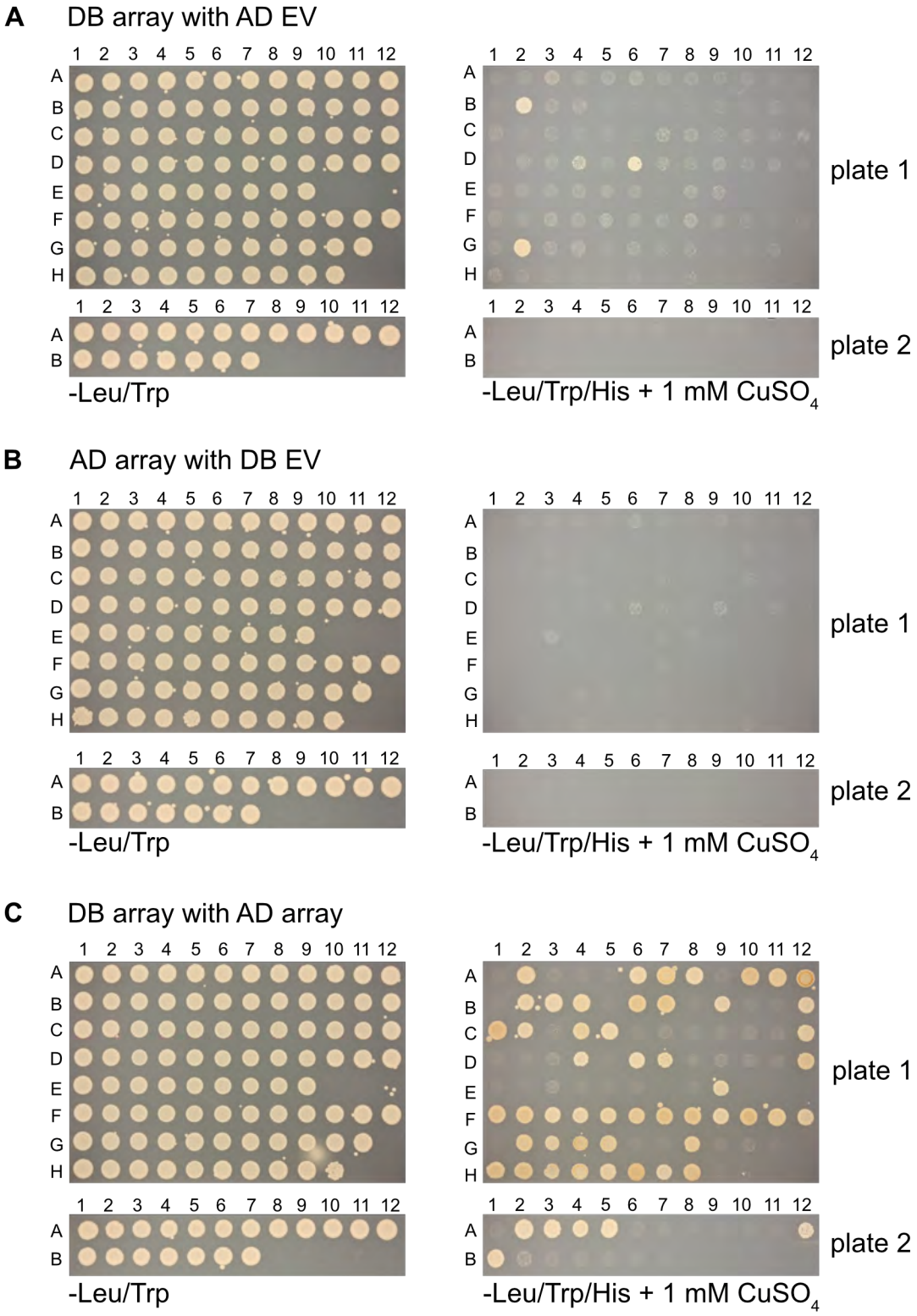
Figure EV2 - Retest of iBFG-Y2H interactions with *L. pneumophila* effectors